

Rates of erosion and their implications for exhumation

D. W. BURBANK*

Institute for Crustal Studies, University of California, Santa Barbara, CA 93106, USA

ABSTRACT

At time-scales of 10^2 to 10^5 years, erosion by rivers, landslides and glaciers can exceed 5 mm/y. Sustained denudation at these rates is sufficient to account for many of the rapid rates of unloading or cooling that are revealed by geobarometric or thermochronologic studies. Because feedbacks exist among many surface processes, determinations of erosion rates on a few geomorphic processes can be adequate to estimate mean rates across an entire landscape. Rates of fluvial and glacial incision exert a dominant control on landscape lowering, because these rates set the local base level and modulate the flux from adjacent hillslopes. When rates of deformation are sufficiently rapid and sustained, a collisional orogen approaches a dynamic equilibrium or topographic steady state. Due to variations in erosion rates as a function of Late Cenozoic climate changes, such a steady state should be defined at time-scales longer than one climate cycle. During dynamic equilibrium, the geomorphic system displays a predictable configuration of interacting rivers, hillslopes and glaciated process zones. A dynamic equilibrium appears to prevail near Nanga Parbat, Pakistan, and the Southern Alps of New Zealand, where spatial variations in geomorphic erosion rates mimic variations in bedrock cooling rates at time-scales of 10^6 y.

KEYWORDS: erosion, exhumation, denudation, Nanga Parbat, Southern alps, New Zealand.

Introduction

RECENT advances in thermochronometry and in petrologically based determinations of the T - P histories of rocks have led to increasingly detailed and reliable reconstructions of P - T - t pathways for rocks now found at the Earth's surface. Some of these data require both rapid and sustained decreases in the pressures experienced by rocks formerly deep in the crust. When these rates of unloading exceed a few mm/y, pressure reductions of this magnitude have commonly been attributed to tectonic exhumation through extensional processes in the upper crust. Indeed, in extensional terranes around the world, there exists abundant support for such tectonic mechanisms of unloading (Wernicke, 1992), and even within many convergent orogens, the evidence for extension during overall contraction is unambiguous (Burchfiel *et al.*, 1992; Platt, 1986). In these interpretations of the driving mechanisms for

observed decompression, erosion by surface processes has been usually relegated to a minor or negligible role. Widespread perceptions that erosion rates are unlikely to exceed 1 mm/y imply that surface processes are incapable of producing the observed rapid rates of unloading.

The overall purpose of this paper is to argue that, for rates up to ~10 mm/y, erosion may dominate the unloading process and to discuss ways in which such an erosional system may function. Commonly, geomorphic studies document an erosion rate for only one or two processes across a landscape. To interpret the significance of such rates for an entire landscape, it is important to understand the linkages existing among different surface processes. Such linkages are the initial focus of this paper, because they provide a key context for understanding other geomorphic results. These linkages imply that rates of erosion attributable to ostensibly separate processes may, in actuality, be closely coupled. For example, the rates of denudation due to conversion of bedrock to regolith, soil creep, and shallow landsliding on soil-mantled slopes are

* E-mail: burbank@crustal.ucsb.edu

interdependent. A conceptual model for several such linkages is presented here. Second, the results of recent studies are used to argue that erosion due to surface processes does, in fact, occur at rates that are sufficiently rapid to account for many reconstructed rates of unloading. Recent quantification of surface-process rates indicates that bedrock erosion rates in rapidly deforming areas can exceed several mm per year. The evidence that several different mechanisms of erosion can sustain such rates is reviewed here. Finally, in the face of sustained high rates of deformation, some combination of erosion and extension rates are likely to balance rates of rock uplift within an orogen and to create a 'steady-state' orogenic belt. Some conceptual models for steady state and the types of evidence that can be gathered to support a steady-state interpretation are discussed.

Exhumation rates inferred from bedrock data

Combinations of geobarometers with geochronometers can be used to define time-pressure histories for rocks. If reasonable assumptions are made to convert pressure to depth below the surface, then changes in the depth of a rock beneath the surface through time can be deduced and an exhumation history can be reconstructed. In the past few decades, improved geobarometric calibrations and increasingly precise dating techniques have enabled the development of ever-more-detailed exhumation pathways. Many rates of exhumation are also estimated from temperature-time paths for which a geothermal gradient is either established or assumed and is subsequently used to convert closure temperatures to depth.

Documented rates of rapid orogenic exhumation commonly fall into two categories: those derived from upper and mid-crustal rocks; and those derived from ultrahigh- P terranes. Exhumation rates from upper and mid-crustal rocks are commonly in the range 1–10 mm/y (Table 1). Many of these rates were determined for collisional mountain belts, some of which preserve evidence of syntectonic extension. In contrast, the most extreme exhumation rates are commonly associated with rocks from ultrahigh- P terranes, where unloading rates that approach plate motion rates have recently been documented (Amato *et al.*, 1999; Rubatto and Hermann, 2001). These rates can be as high as 20–30 mm/y (Table 1). These terranes typically

comprise rocks that were rapidly decompressed from depths of ~100 km to depths of 20–40 km, after which the rates of exhumation commonly decreased by ≥ 10 fold to rates of <5 mm/y.

Linkages among erosional mechanisms

Fluvial systems

Local base level can be conceived of as the lowest topographic point within any given sector of a landscape. Whereas ultimate base level is typically the ocean or a closed topographic depression, local base level can be defined in the context of the mosaic of rivers, hillslopes and glaciers that constitute mountainous landscapes. Within any catchment, the local base level can be represented as the longitudinal valley profile: each point along the profile defines the local base level for all points upstream (or tributary) to that point, including the adjacent hillslopes (Horton, 1945; Bull, 1991). In most settings, there are only two surface processes that commonly can define the local base level: the actions of rivers and glaciers. Other surface processes may influence whether the beds of rivers or glaciers are aggrading or degrading and whether the local base level, as set by the rivers or glaciers, is rising or falling through time at particular point or time. Such processes, however, do not directly set the local base level. For example, an increased sediment flux from adjacent hillslopes can force a river to aggrade, thereby increasing the local base level. Nonetheless, it is the vertical position of the river or glacier, rather than the shape of the adjacent hillslope, that directly defines the relevant local base level.

Erosion occurs on non-glacial hillslopes via conversion of bedrock to regolith, downslope creep of the regolith, rain splash, shallow overland flow, various biologically mediated processes, such as tree-throw and animal burrowing, and both shallow- and deep-seated landsliding. Rates of all these processes increase with increasing hillslope gradients (Montgomery and Dietrich, 1994) or curvature (Heimsath *et al.*, 1997, 1999). There is an obvious and fundamental control on the angle of a hillslope exerted by the river channel at the base of the hillslope (Fig. 1), because rates of channel lowering (or aggradation), rates of hillslope lowering, and changes in hillslope angles are all linked. The hillslope gradient can be defined either as the mean slope proximal to the channel or as the mean slope from the channel to the bounding drainage divide. If the

TABLE 1. Exhumation rates based on geobarometry and thermochronology.

Location	Exhumation rate	Magnitude of lithostatic load removed	Duration of unloading event	Shallowest calibrated depth ¹	Age at time of shallow depth ²	Reference
Southern Alps, New Zealand	6–10 mm/y	10–20 km	2 m.y.	0 km	0 Ma	Tippett and Kamp (1995)
Nanga Parbat, Pakistan	5–7 mm/y	15–20 km	3 m.y.	0 km	0 Ma	Zeitler <i>et al.</i> (2001)
European Alps (Dora Maira)	5 mm/y	10 km	~2 m.y.	8 km	30 Ma	Rubatto and Hermann (2001)
Crete, Greece	4–8 mm/y	25 km	4–6 m.y.	4 km	15 Ma	Thomson <i>et al.</i> (1999)
Nepalese Himalaya	4–5 mm/y	25 km	4–6 m.y.	0 km	0–2 Ma	Harrison <i>et al.</i> (1997)
K2, Karakoram	3–6 mm/y	>3 km	0.5–2 m.y.	4 km	2 Ma	Foster <i>et al.</i> (1994)
European Alps (Zermatt-Saas)	3 mm/y	6 km	20 m.y.	9 km	13 Ma	Amato <i>et al.</i> (1999)
Basin and Range, USA	2–4 mm/y	10–15 km	3–5 m.y.	0 km	15 Ma	Foster and John (1999)
Irian Jaya, Indonesia	1.7 mm/y	>4 km	~2 m.y.	0 km	0 Ma	Weiland and Cloos (1996)
Denali, Alaska	1.2 mm/y	6 km	4 m.y.	0 km	0 Ma	Fitzgerald <i>et al.</i> (1995)
Olympic Range, Washington	1.2 mm/y	9 km	11 m.y.	4 km	7 Ma	Brandon <i>et al.</i> (1998)
Ultrahigh- <i>P</i> rocks						
European Alps (Dora Maira)	34 mm/y	75 km	~2 m.y.	40 km	33 Ma	Rubatto and Hermann (2001)
European Alps (Dora Maira)	16 mm/y	17 km	~1 m.y.	18 km	32 Ma	Rubatto and Hermann (2001)
European Alps (Zermatt-Saas)	10–26 mm/y	65 km	2.5–7 m.y.	25 km	38 Ma	Amato <i>et al.</i> (1999)
Kokchetav, Kazakhstan	~20 mm/y	160 km	7 m.y.	15 km	528 Ma	Hacker <i>et al.</i> (in review)

¹ Reconstructed depth of the control point beneath the palaeosurface

² Age at the time rocks were at the shallow control-point depth

rate of channel incision is greater than the rate of lowering of the drainage divide or of the hillslope

adjacent to the channel, the hillslope gradient will increase.

Slopes controlled by soil production rates

Creep, rainsplash erosion and various biologically mediated processes are commonly modelled as diffusive erosion processes (Andrews and Hanks, 1985; Beaumont *et al.*, 1992; Hanks *et al.*, 1984). Traditionally most numerical models have defined diffusive sediment transport (q_s) with a linear dependence on slope (S):

$$q_s \propto S \quad (1)$$

This approximation (Fig. 2a) is consistent with the observation that the gradient of many soil-mantled slopes typically increases away from the drainage divide. The tendency for slopes to

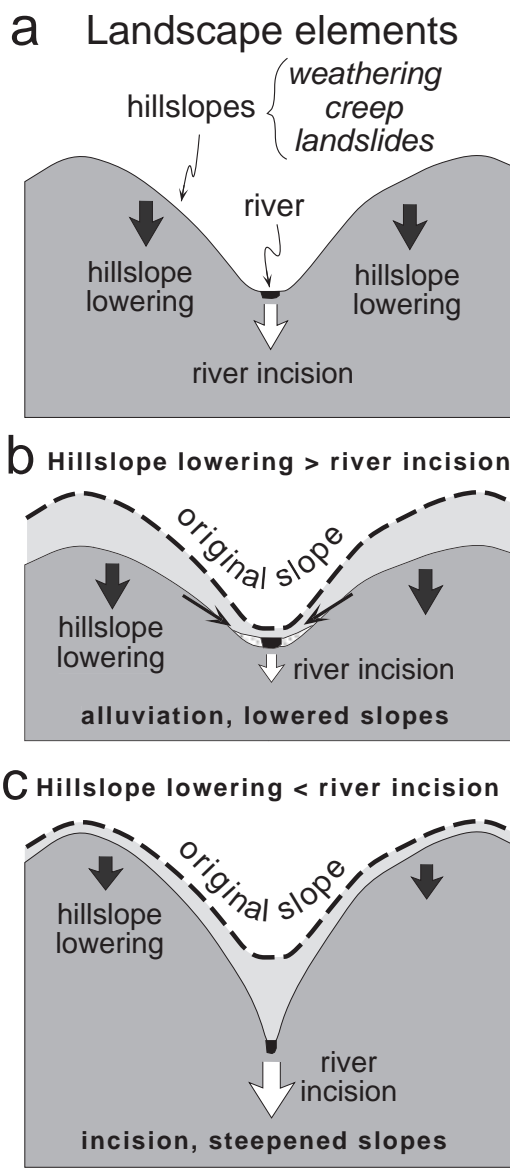


FIG. 1. (a) Linkage between local base level set by a river, adjacent hillslopes, and competing rates on hillslopes and channels. (b) When the rate of channel incision is greater than the rate of lowering of crest of hillslope, the mean hillslope angle steepens, and sediment fluxes that are slope-dependent should increase. (c) Alternatively, if hillslope lowering is greater than channel incision, hillslope gradients will decrease.

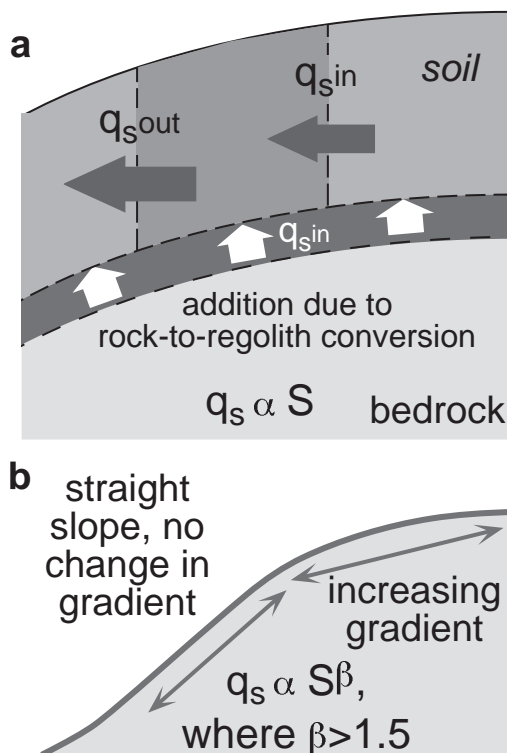


FIG. 2. Model for hillslope sediment production and transport. (a) Sediment flux increases downslope due to additions of weathered bedrock at the base of the soil-regolith. Increased sediment fluxes are accommodated by increased slope gradients. (b) Observed hillslope profiles have straight segments that are more consistent with a non-linear transport rate.

RATES OF EROSION AND EXHUMATION

become more linear farther downslope, however, suggests the sediment flux may show a power-law dependence on slope (Roering *et al.*, 1999),

$$q_s \propto S^\beta \quad (2)$$

where $\beta > 1.5$. The strong slope-dependence of either sediment-flux rule underlines the sensitivity of erosion rates to slope angles.

As hillslope gradients increase, landsliding becomes a more important erosional process. Commonly shallow landslides only involve regolith. Therefore, the rate of sediment delivery by such landslides is limited by the rate at which rock is converted to regolith. In fact, the maximum rate of sediment transport due to both shallow landsliding and diffusive hillslope processes, such as creep, will be set by the rock-to-regolith conversion rate. Therefore, in such landscapes, it is sufficient to quantify the regolith production rate in order to define the upper limit of hillslope erosion. Because this rate is sensitive to the thickness of the overlying soil (Heimsath *et al.*, 1997; Rosenbloom and Anderson, 1994), there also exist negative feedbacks in the regolith production-hillslope transport system. Regolith production rates are greatest beneath a relatively thin soil or on slopes with high curvature (Heimsath *et al.*, 1999). Consequently, if the rate of sediment removal from a hillslope is slower than the regolith production rate, the regolith will thicken and its rate of production will diminish until it approaches a balance with the rate at which soil is transported downslope.

Slopes controlled by rock strength

In contrast to diffusive hillslopes, sediment delivery by bedrock landslides is independent of rock-to-regolith conversion rates, and is instead controlled by bedrock strength, which is itself a function of rock type, fracture density, bedding geometry, pore pressure, and seismic shaking, among other factors. Landslides will occur when the shear stresses exceed the hillslope strength (Selby, 1982; Allen, 1997):

$$\rho_r g h \sin \alpha \cos \alpha > C + (\rho_r - p_w) g h \cos \alpha \tan \phi \quad (3)$$

where ρ_r rock density, g = gravitational acceleration, h = depth to the potential glide plane, α angle of the potential rupture surface, C = cohesion, p_w = pore water pressure, and ϕ angle of internal friction. As would be expected, the rate of landsliding is strongly slope dependent, such that the frequency of landsliding typically increases as hillslope gradients steepen. Due to this slope dependence, the bedrock landsliding rate is commonly linked to the rate of channel incision and base-level lowering (Fig. 1). It is easy to imagine, however, that, for any combination of the variables listed above, there is some critical slope angle above which the shear stresses will exceed the hillslope strength, such that landsliding is likely to occur. This 'threshold slope angle' is of great significance for the shape of the landscape (Fig. 3), because it sets the upper limit for hillslope gradients (Burbank *et al.*, 1996; Schmidt and Montgomery, 1995, 1996). Below the threshold angle, increasing rates of channel

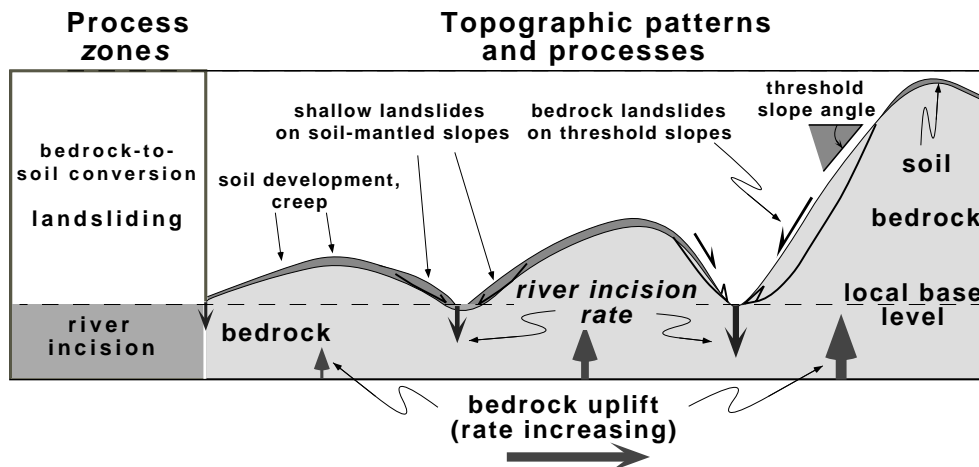


FIG. 3. Dominant hillslope processes in response to increasing rates of river incision.

incision and local base-level lowering will increase hillslope gradients, whereas once that threshold slope angle is attained, the hillslope gradient will be independent of the rate of channel incision and should instead hover around the critical angle for slope failure (Fig. 3). For cohesionless materials, this threshold angle or angle of repose is commonly $\sim 30^\circ$, whereas greater cohesion and strength will yield higher threshold angles. Although rock strength permits local hillslopes to exceed 50° in active orogens, in many rapidly denuding ranges, such as the Himalaya, the average hillslope angle commonly lies near 30° (Burbank *et al.*, 1996).

Hillslope-channel linkages

The possibilities for negative feedbacks in this linked hillslope-channel system are clear. Increased sediment fluxes off steepened hillslopes deliver a larger sediment load to the channel. In order to continue incising, the channel must remove this extra sediment. To the extent that this sediment flux exceeds the transport capacity of the river, the rate of channel incision will diminish, and aggradation may occur. Such aggradation will decrease the adjacent hillslope gradients and reduce the slope-dependent sediment flux, thereby increasing the possibility that the stream will be able to remove the sediment delivered to it and begin incising its bed again. Such negative feedback loops suggest that, over time, average hillslope gradients should become adjusted to the mean rates of river incision, such that the average sediment delivery from the hillslope matches the transport capacity of the river that is in excess of that needed to transport the load delivered from upstream.

One might imagine that as the flux from hillslopes decreases, the rate of bedrock incision would increase. One logical deduction from this is that rivers would incise most efficiently in the absence of any sediment flux from adjacent hillslopes. Contrary to this expectation is the fact that water alone is not a very effective erosion agent. Sediment carried by rivers provides 'tools' that deliver highly focused energy to the bed of the river as they roll or saltate along the bed. Because this energy drives fluvial erosion, the presence of tools is a key control on incision (Sklar and Dietrich, 1998). If there is too much sediment, the bedrock is covered and cannot be eroded, whereas if there are too few tools, the erosion process is inefficient. Thus, for the most efficient erosion, there needs to be a balance

between the rate at which tools are supplied to the river and the rate at which they can be transported.

Glacial systems

Local base-level can also be set by glaciers, which sculpt valley bottoms and influence the gradients of adjacent hillslopes. Glaciers, however, obey a different (and less well known) set of rules than do rivers. For example, rivers do not incise their beds significantly below base level. Knickpoints in river profiles that are created by drops in base level are systematically propagated upstream (Howard *et al.*, 1994; Schumm *et al.*, 1987; Seidl *et al.*, 1994; Slingerland and Snow, 1988). In contrast, as evidenced by fiords and innumerable glacial lakes, glaciers can excavate hundreds of meters below local base level. Whereas little is known about the lateral propagation of steepenings (or 'knickpoints') in glacial profiles, it is clear that many of these do not originate near the toe of a glacier and propagate upglacier in a pattern analogous to knickpoint migration in rivers. Instead, these knickpoints in longitudinal profiles appear related to the average position of glacial snowlines (Porter, 1989) and to the planform geometry of converging glaciers (MacGregor *et al.*, 1998). The surface of the glacial ice or the deglaciated floor of a glacial valley sets the local base level for adjacent hillslopes. During glacial times, advancing and thickened glaciers commonly widen valley bottoms and may also buttress adjacent valley walls (Harbor *et al.*, 1988; Whipple *et al.*, 1999). Both of these processes can steepen hillslope angles adjacent to a glacier (Whipple *et al.*, 1999). Because glaciers experience greater fluctuations in thickness than do rivers, the average gradients of hillslopes bounding glaciated valleys will vary more markedly during a glacial-interglacial cycle than will those of fluvial hillslopes. These glacial hillslopes might, therefore, be expected to switch more completely and frequently between stable and unstable slope domains with respect to landsliding. The observation of large-scale bedrock landsliding within decades of deglaciation during the 1900s supports the hypothesis that removal of the buttressing effect of glacial ice enhances slope instabilities (Meigs, 1998).

Delivery of material from adjacent valley walls has a different impact on glaciers than it does on river systems. Whereas enhanced sediment fluxes from hillslopes into rivers may cause them to

RATES OF EROSION AND EXHUMATION

aggrade, glaciers are far less sensitive to sediment fluxes on to their upper surfaces. The high viscosity of ice permits nearly all grain sizes to be transported readily. As with rivers, a flux of rocks to the surface may provide 'tools' that promote basal erosion, if the rocks fall into the accumulation zone where glacial flowlines carry these rocks downward to the ice-bedrock interface (Hallet, 1979). If rockfalls occur in the ablation zone, the resulting blanket of debris can reduce the rate of melting and promote the advance of the glacier (Clark *et al.*, 1994). Such advances are likely to enhance glacial erosion.

Rates of erosion

As described above, important mechanisms by which erosion occurs include conversion of bedrock to regolith, creep, landsliding on soil-mantled slopes, bedrock incision by rivers, bedrock landsliding, and glacial erosion. The advent of cosmogenic radionuclide exposure dating techniques has ushered in a new era in which direct dating of bedrock weathering rates is possible (Nishiizumi *et al.*, 1993). Recent cosmogenic nuclide studies of bare bedrock in both alpine and desert settings suggest that rates of weathering of exposed bedrock (grain-by-grain erosion or dissolution of the surface) are commonly on the order of 5–20 $\mu\text{m}/\text{y}$ (Bierman, 1994; Small *et al.*, 1997), although they may approach 300 $\mu\text{m}/\text{y}$ (Heimsath, 1999). Rock-to-regolith conversion rates have been shown to be as high as 100–300 $\mu\text{m}/\text{y}$ (Heimsath *et al.*, 1997, 1999). Because all of these studies document erosion rates that are fractions of a mm/y, it is clear that these processes are incapable of producing the rapid unloading indicated by some *P-T-t* studies. Similarly, because maximum erosion rates via processes such as creep or landsliding on soil-mantled slopes are controlled by the rate of regolith production, these processes are also incapable of producing rapid, long-term rates of erosion or unloading. Consequently, there are only three major surface processes (fluvial incision, bedrock landsliding, and glacial erosion) that need to be considered as possible agents for rapid erosion.

Fluvial erosion

If the sediment load transported by a river is known, a mean denudation rate for the upstream catchment can be calculated. Although the

sediment load comprises bedload, suspended load, and dissolved load, erosion by rivers has commonly been estimated using suspended sediment loads (Milliman, 1997; Milliman and Syvitski, 1992). In many large rivers, observations that the bedload and dissolved load account for <15% of the total load appears to justify reliance primarily on the suspended load. Rates that are derived from such calculations, even for Himalayan rivers, commonly are <1 mm/y when averaged over entire catchment (Fig. 4). Several factors, however, complicate the interpretations of these data with respect to erosion within active orogens. Most of these estimates come from the mouths of rivers, where they represent averages over an area that is much larger than the more rapidly eroding mountains which commonly make up only a small fraction of the catchment. These river-mouth data also ignore any storage that may take place in basins intervening between the mountains and the delta. For example, recent comparisons of the isotopic signature of suspended sediments with that of bedload and floodplain strata in the Himalayan foreland (Galy and France-Lanord, 2001) suggest that only ~50% of the total load is reaching the river's mouth as suspended load. In addition, some mountainous catchments may have a much higher bedload component (up to 50%) than is commonly assumed. Although the total sediment load is notoriously difficult to quantify in rapidly denuding mountainous catchments, the erosion rates estimated from suspended sediment loads (Fig. 4) should be regarded as minimum rates that could be several times higher within active orogens.

The fluvial erosion estimates described above represent an average denudation across an entire catchment above the point where the suspended sediment was collected (Fig. 4). Because rivers actually occupy only a very small fraction of most landscapes, these mean rates primarily indicate average hillslope denudation rates. As such, they provide little direct quantification of how rapidly rivers are incising into bedrock. Yet, given that the rivers set the local base level for adjacent hillslopes and ultimately determine how rapidly these hillslopes can erode, direct measures of river incision are illuminating.

The key mechanisms whereby rivers incise their beds are hotly debated at present and are a focus of current geomorphological research (see reviews in Tinkler and Wohl, 1998). Direct measurements of river incision rates into

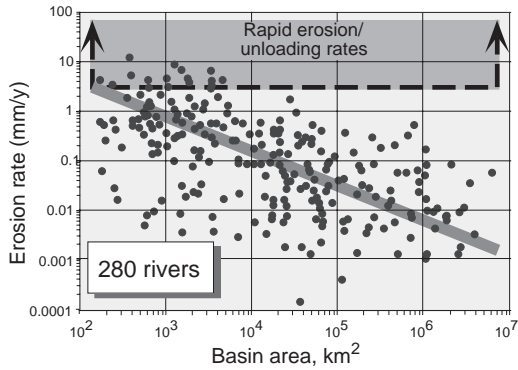


FIG. 4. Rates of erosion averaged over entire catchments and based on suspended sediment loads in rivers. The trendline indicates that rates tend to increase for smaller catchment sizes. Only a few catchments of $<10^4$ km² display rates that exceed a few mm/y. (Modified after Milliman and Syvitski, 1992).

other preserved features, such as potholes, that a river imprinted on the landscape as it incised its bed. Along the gorges of some rapidly incizing rivers, remnants of multiple strath terraces are etched on the valley walls. In order to use these to determine incision rates, the time at which the river abandoned the strath surface must be determined. When combined with the strath's present height above the river, an average incision rate can be calculated (Fig. 5).

Determining the time of abandonment of the strath and the initiation of incision is commonly difficult. When a veneer of fluviably bedded material has been deposited on top of the strath prior to the beginning of incision, standard geomorphic-chronologic approaches, such as radiocarbon dates on incorporated organic material or luminescence dates on windblown and lacustrine silts, can be used to place a limit on the time of incision. In some situations, well preserved, fluted, and potholed strath surfaces provide a robust indication of former river levels, but are devoid of any cover and are not amenable

bedrock, however, can be determined using strath terraces (river terraces incised into bedrock) or

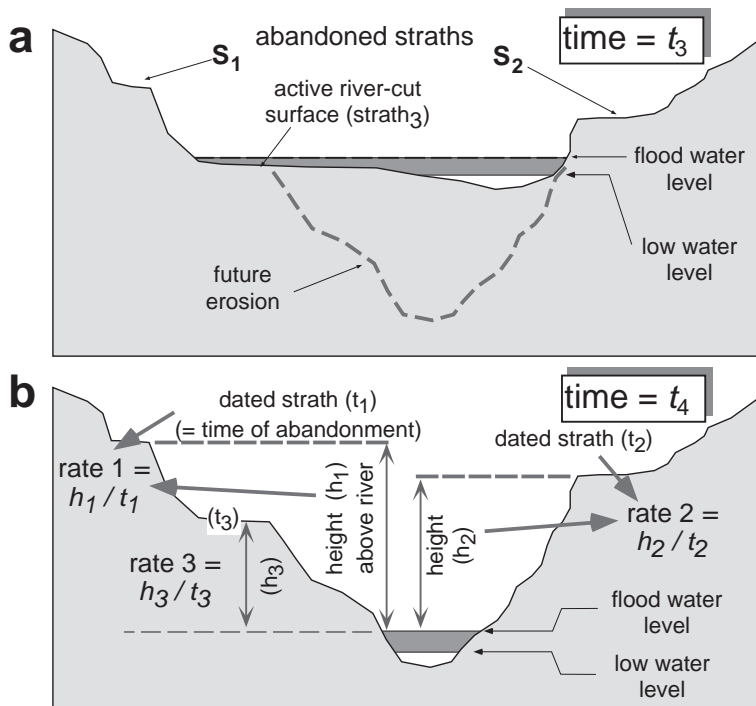


FIG. 5. Scheme for calculating river incision rates from strath terraces. (a) At time t_3 , two previously formed strath terraces (s_1 , s_2) are preserved and a third (s_3) is being formed. Erosion that will occur subsequent to this time step is shown by the dashed line. (b) Calculation of rates of river incision at time t_4 . A separate rate can be calculated using the height and time of abandonment of each strath.

RATES OF EROSION AND EXHUMATION

to standard dating techniques. A decade ago, such surfaces would have been considered undatable. But now, cosmogenic radionuclide chronologic techniques provide a powerful tool that can yield estimates of the time since the strath was abandoned (Nishiizumi *et al.*, 1993). Specifically, if a pristine abandoned surface is available, then cosmogenic nuclide abundances can indicate the elapsed time since the surface was first exposed to extensive cosmic ray bombardment. Several assumptions enter into interpretations of cosmogenic dates: (1) The erosion that created the strath is assumed to have removed at least 1–2 m of rock, such that there is no significant inheritance of cosmogenic nuclides from prior to creation of the strath. The geometry of most strath surfaces indicates that this assumption is likely to be valid. (2) The time required to create the strath itself is assumed to have been short in comparison to the time since the river abandoned the strath. Consistent ages at multiple sites on a single strath suggest that they form in $\sim 1\text{--}5 \times 10^3$ years (Leland *et al.*, 1998). Thus, for most pre-Holocene straths, this assumption should be valid. (3) The surface of the strath is assumed to have experienced no significant erosion ($< 1\text{--}5$ cm) since abandonment. Preservation of polished, fluted surfaces can validate this assumption. (4) Since abandonment, the strath surface is assumed to have remained exposed and unshielded from cosmic radiation. If landslides or other rock debris had been present on the surface in the past, these would have shielded the strath surface from radiation, and the exposure age of the surface would be younger than the actual age. Thus, the choice of what strath to sample should include an assessment of the geomorphic history of the site.

When these assumptions are met, formerly intractable incision rate calculations in large mountain ranges can be attempted. For example, in the Indus River gorge in the vicinity of Nanga Parbat, northwest Pakistan, well preserved strath surfaces lie from 50 to > 400 m above the present surface of the river (Burbank *et al.*, 1996). In these straths, the measured concentrations of cosmogenic nuclides of ^{10}Be and ^{26}Al yield ages as old as ~ 70 ka for the time of abandonment of individual terraces. Variations in the height and ages along the river yield striking variations in incision rates (Fig. 6). Most importantly as indicators of the importance of erosional processes during unloading, the rates of incision into the igneous and metamorphic rocks of the

High Himalaya are as high as 10 mm/y (Burbank *et al.*, 1996). Such rates are comparable to the rapid unloading rates that are deduced elsewhere from some *P-T-t* data sets, e.g. Guillot *et al.* (1999).

The significance of rates that are sustained over only $1\text{--}8 \times 10^4$ y might be questioned. Although those rates that span the past 20 ky or more have at least experienced full glacial and interglacial conditions, they sample only a fraction of a single, typical climate cycle (~ 100 ky). Given the time-scales of orogenesis or of the development of topography at the scale of mountain ranges (Anderson, 1994; Whipple *et al.*, 1999), rates over intervals of $< 10^5$ y might seem irrelevant or at least lacking in a meaningful temporal context. Consider, however, the geomorphic implications of rates of rock uplift or river incision of ≥ 5 mm/y. A strath formed at river level only 100 ky ago would now be located ≥ 500 m above the valley bottom! In 500 ky, over 2.5 km of river incision and rock uplift would occur. With the possible exception of uplifted coastal terraces in a few select locations (Bull and Cooper, 1986), the opportunity for preservation of pristine geomorphic features is vanishingly small in such rapidly deforming terrains at time scales $> 2\text{--}4 \times 10^5$ y. For example, in the Indus gorge (Fig. 6), straths preserved ~ 400 m above the modern river are only ~ 30 ky old (Burbank *et al.*, 1996). At present, these straths are fragments of formerly more extensive fluvial surfaces which have been removed or buried by landslides as they were elevated hundreds of metres above the valley floor. Hence, in rapidly eroding terrains, the interval over which rates can be practically measured is commonly limited to $< 5\text{--}10 \times 10^4$ y. Despite the relative brevity of this time frame, these rates demonstrate that hundreds of metres of rock can be eroded at rapid rates by river incision. Given the persistence of these processes through climate cycles, there is good reason to expect that they would yield sustained incision rates of > 5 mm/y: equivalent to pressure decreases of 1–2 kbar per million years as documented for metamorphic rocks during Himalayan-style orogenesis (Guillot *et al.*, 1999; Harrison *et al.*, 1997).

Mass wasting

Although mass wasting can occur through numerous mechanisms, such as gelifluction or debris flows, only two types of mass wasting are

considered here to be of significance as agents of rapid erosion: bedrock landslides and massive rockfalls. Whereas the rate of erosion by shallow landslides involving only regolith is limited by the rate of production of regolith and is, therefore, <1 mm/y (Heimsath *et al.*, 1997), erosional fluxes due to bedrock landsliding have no such limitations and could, theoretically, attain very high rates. The difficulty in the past has been in finding appropriate means to quantify the rate of sediment delivery by landslides. Even if the age of each landslide in a mountainous area were somehow definable, the full volume of original landslides is rarely preserved through time. Thus most derivations of fluxes based on preserved volumes would tend to underestimate the actual total. In landscapes where erosion by landslides dominates the sediment flux, there are commonly hundreds to thousands of landslide scars and accumulations of landslide debris. Dating all of these features becomes an intractable task.

Many of these limitations have been circumvented by an innovative approach to quantifying landslide fluxes (Hovius *et al.*, 1997). Through examination of multiple sets of aerial photographs of a region, it is possible to use a younger set of photographs to define the number and size of the landslides that have occurred since an older set of photographs was taken. A compilation of the statistics of landslides in the fixed time slices that are dictated by the intervals between aerial photographs yields data on magnitude-frequency relationships of landslides (Fig. 7). In such studies, the frequency per km² per year of landslides greater than a given area (A_c) is

plotted as a function of landslide area (Fig. 7). In most such studies to date, the data define a power-law function in which the slope of the best-fit line yields the exponent ($-\beta$) for the magnitude-frequency relationship. When such a relationship is valid, the number of slides of magnitude equal or greater than area $A_c[n_c(A \geq A_c)]$ is expressed as:

$$n_c(A \geq A_c) = \kappa(A_c/A_r)^{-\beta} A_r \quad (4)$$

where A_r is a reference area, and κ is the intercept of the regression when $A_r = 0$ (Hovius *et al.*, 1997).

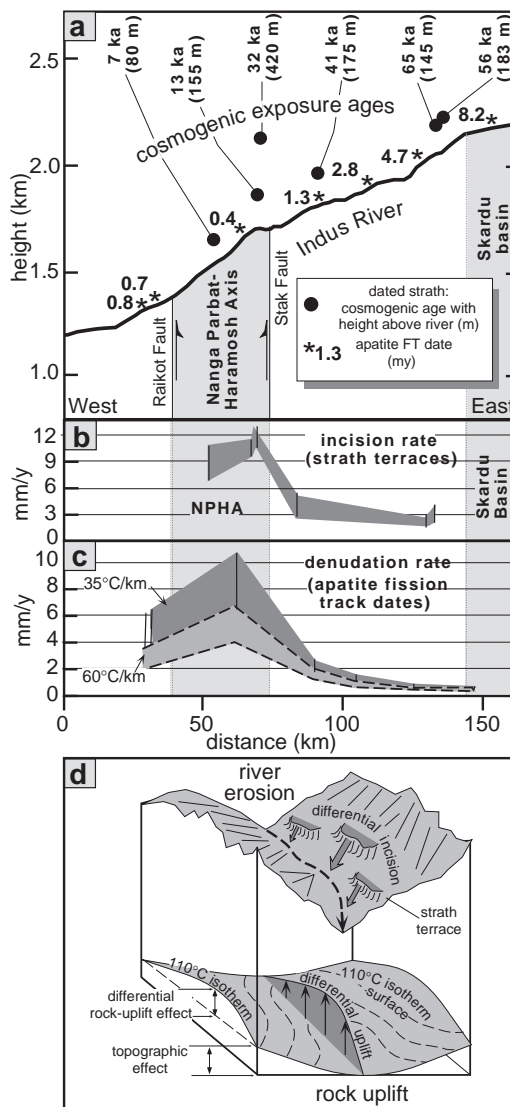


FIG. 6. (a) Cosmogenic nuclide exposure ages, elevations of strath terraces, and apatite fission-track ages as a function of distance and altitude along the middle Indus gorge in the vicinity of Nanga Parbat. Fission-track ages from Zeitler (1985) and A. Blythe (pers. comm., 1999). (b) Bedrock incision rates calculated from dated straths. (c) Denudation rates derived from apatite fission-track (AFT) dates as calculated for two different geothermal gradients. For location of transect, see Fig. 11. Modified from Burbank *et al.* (1996). (d) Sketch illustrating the relationship between spatially variable rock-uplift rates (as calculated from AFT dates) that are matched by spatially variable incision (as calculated from the differential height of strath terraces). Rates based on AFT dates represent the time since passage through the 110°C isotherm. This isothermal surface is warped (indicated by dashed contours) due to the effects of both topographic and differential uplift.

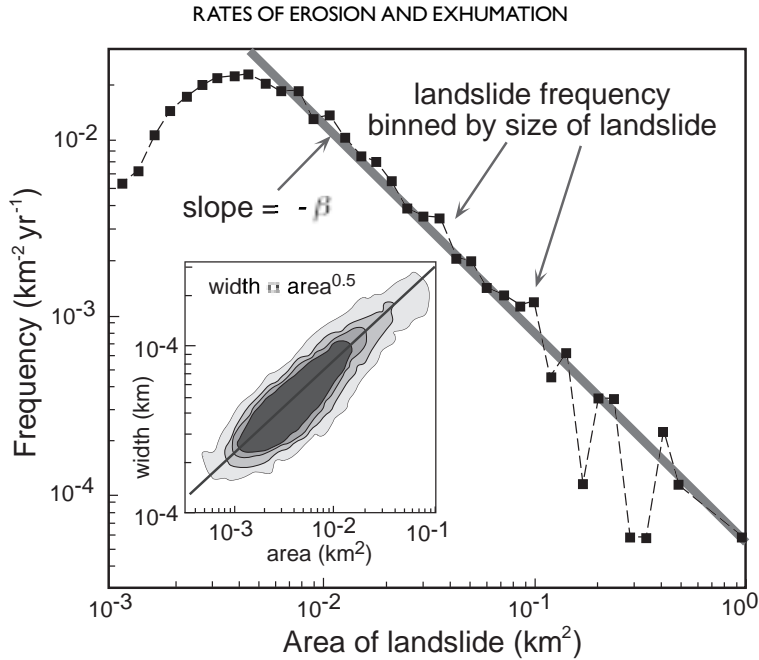


FIG. 7. Magnitude-frequency relationship for landslides on the western flank of the Southern Alps, New Zealand. Inset shows landslide width vs. landslide area. Modified after Hovius *et al.* (1997)

Translating the frequency-magnitude relationship into a sediment flux from landslides requires several steps. First, the areal extent of a landslide has to be converted to volume. This has been done (Hovius *et al.*, 1997) by relating landslide area to its measured width (L) and then relating the width to mean depth, commonly, estimated as 5% of the width (Ohmori, 1992). Second, although the conversion to volume permits a flux to be calculated directly, this flux represents an average only over the sampled interval. Most commonly, this interval does not encompass infrequent, large events. The magnitude-frequency relationship yields a prediction of how often larger events should occur over longer time spans (Fig. 7), whereas the value of the exponent β determines whether the sediment flux is dominated by a few large landslides or by far more numerous, but smaller ones. For $\beta < 1.5$, large landslides dominate, and the total flux can be estimated (Hovius *et al.*, 1997) as:

$$V = \frac{2\beta\epsilon\kappa L_1^{3-2\beta}}{(3-2\beta)} \quad (5)$$

where ϵ = ratio of landslide width to depth, L_1 = width of the largest topographically permissible

landslide in the area of study. The initial landslide study of Hovius *et al.* (1997) in the Southern Alps of New Zealand was targeted at an area where previous fission-track studies had defined regional patterns of cooling with respect to the Alpine Fault (Tippett and Kamp, 1993, 1995). These fission-track data suggest that oblique convergence between continental blocks within the Pacific and Australian plates has resulted in a systematic spatial variation of rock uplift and erosion across the South Island of New Zealand (Kamp and Tippett, 1993). Cooling ages of < 1 m.y. near the Alpine Fault have been interpreted to indicate rapid unroofing there at rates > 5 mm/y (Tippett and Kamp, 1993). This zone of inferred rapid denudation lies on the western flank of the Southern Alps. The landslide study of Hovius *et al.* (1997) in part of this same region yielded the remarkable result that the sediment flux due to landsliding represents an average erosion rate of 9 ± 4 mm/y. As with the fluvial incision rates described above, erosion rates of this magnitude are compatible with many of the more rapid rates of unroofing defined in metamorphic terrains.

Although similar landslide studies using repeat aerial photography have only been completed in a

few areas (Burbank *et al.*, 1998; Hovius *et al.*, 2000), this approach appears to hold great potential for quantification of fluxes due to landsliding. It avoids many of the difficulties in assigning ages to geomorphic features, like landslides or straths, and in calculating the original volume of older, partially preserved slides. Further work needs to be done to quantify the area-width-depth-volume relationships for landslides, to define the revegetation interval for slide scars (this becomes important if the time between photographs is long with respect to the revegetation time), to explore the sensitivity of the frequency-magnitude relationships, to evaluate any anthropogenic acceleration of landslide frequency, and to define the appropriate uncertainties to attach to flux estimates. Despite these unresolved issues, this new approach opens the possibility of estimating landslide fluxes in any range for which repeat aerial photographs or high resolution satellite images are available.

Glacial erosion

Obscured by overlying ice and glacial till, erosion at the base of a glacier is difficult to observe directly or to quantify. Most studies have utilized the flux of sediment carried either by subglacial streams, within glacial ice, or on the upper surface of glaciers to estimate the rate of erosion by glaciers. Measurements of sediment loads in glacial streams are particularly difficult, because a large fraction of the load may move as bedload. Some studies of sediments emerging from the glacial snout have deduced that the sediment flux

was proportional to the ice flux (Humphrey and Raymond, 1994) and suggested that glacial erosion rates might scale with the ice flux through the glacial equilibrium line (the steady-state snowline) (Anderson and MacGregor, 1998).

When sediments carried by glacial streams are deposited in proglacial lakes or marine deltas, they can provide a longer term record of sediment fluxes. Such records can integrate deposition over many years and, when their duration is known, they provide an integrated estimate of the sediment flux in glacial environments. Utilizing the volume and age of stored sediments, a recent compilation of data in several alpine areas (Fig. 8) indicates that 20th century glacial erosion rates can exceed several mm/y (Hallet *et al.*, 1996). Interestingly, there is a marked contrast in the rates between relatively quiescent ranges, such as the Alps or in Scandinavia, versus tectonically active ranges in parts of Alaska, central Asia, and New Zealand (Fig. 8). Whereas the former regions yield erosion rates that are typically <1 mm/y, the latter ranges contain numerous glaciers yielding rates exceeding 3–10 mm/y. It is interesting to note that, not only do these rates come from tectonically active ranges, but many of the studied glacier systems are also in regions of high precipitation. One might expect that such high precipitation would drive high ice fluxes through the equilibrium lines of these glaciers and would promote rapid glacial erosion.

Such measurements of erosion rates based on sediment fluxes have at least two likely sources of errors. First, the sediment load measured at the

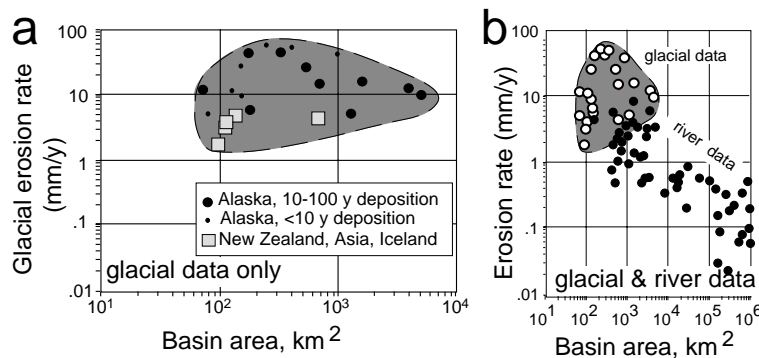


FIG. 8. (a) Glacial erosion rates vs. glacier area in several alpine ranges. Modified after Hallet *et al.* (1996). (b) Comparison of glacial and fluvial erosion rates. Fluvial data from high-relief river systems of Milliman and Syvitski (1992). Note that the glacial erosion rates from Alaska can be 1–2 orders of magnitude greater than fluvial erosion rates for basins of similar size.

RATES OF EROSION AND EXHUMATION

glacial snout or in a lake or delta indiscriminately lumps together material derived from erosion at the base of the glacier and material from the periglacial environment that is commonly delivered by rockfall and avalanches to the glacier surface. If the periglacial contribution to the sediment load were significantly greater than that due to glacial erosion, then the rate of glacial erosion would be overestimated. Second, the leads and lags in the erosion-sediment transport system could produce misleading rates. For example, if sediment eroded over many years is stored beneath a glacier or in the proglacial environment and is only released during deglaciation, then rates measured during deglaciation would tend to overestimate the long-term rate of erosion (Church and Slaymaker, 1989). This may be an explanation for some of the extraordinarily high rates displayed in the Alaskan data (Fig. 8): rates exceeding 10–20 mm/y are strikingly rapid and may be unsustainable. Even if some of these rates are adjusted downward, however, they are comparable to the rapid rates defined for river incision, landsliding, and fluvial erosion (Fig. 8b) and to the rates of unloading inferred from some metamorphic studies (Table 1).

Summary of erosion rates

The preceding description of fluvial, hillslope, and glacial erosion rates clearly indicates that

each of these processes is capable of removing bedrock at sustained rates exceeding 5 mm/y (Table 2). Upon inspection of the global array of rates that have been documented for these processes, it becomes clear that such rapid rates are more exceptional than commonplace. Where rapid rates have been documented, however, they almost always occur in rugged mountains where thermochronologic studies indicate rapid cooling is occurring. The significance of erosional rates such as these is that they obviate the need for extension in the brittle crust to accommodate the rapid rates of unloading that are documented through metamorphic studies. Instead, they suggest that much (or all) of the unroofing could result from erosion by surface processes. Utilization of low-*T* thermochronometers in such settings can lead to similar conclusions. Whereas high-*T* (>300°C) thermochronometers place few limits on denudational mechanisms, lower-*T* thermochronometers can restrict the viable mechanisms that can accommodate unloading. For example, apatite fission-track and (U-Th)/He dates define the time at which a sample cooled below ~110 and 75°C, respectively (Wolf *et al.*, 1998). Given that temperatures of 75–110°C are usually reached within a few km of the surface, any cooling that was experienced by such samples and that was driven by extension would have had to occur on extensional faults within those topmost few km. In the absence of structural

TABLE 2. Erosion rates by surface processes.

Erosion process	Location	Measured characteristic	Rate of erosion	Reference
Bare bedrock weathering	Wind River Range, Wyo.	Cosmogenic isotope abundance	5–20 m/m.y.	Small <i>et al.</i> (1997) Bierman (1994)
Rock-to-regolith conversion	San Gabriel Mtns, Calif.	Cosmogenic isotope abundance	≈350 m/m.y.	Heimsath (1999)
River incision	Indus River, Pakistan	Cosmogenic isotope abundance	5–10 km/m.y.	Burbank <i>et al.</i> (1996)
River incision	Himalayan Foreland	Deformed, dated terraces	10 mm/y	Lavé and Avouac (2000)
Bedrock landsliding	Southern Alps, New Zealand	Frequency magnitude data	5–15 km/m.y.	Hovius <i>et al.</i> (1997)
Glacial erosion	Alaska, New Zealand, Asia	Sediment volumes, reported rates	1–30 km/m.y.	Hallet <i>et al.</i> (1996)
Glacial erosion	Nanga Parbat	Glacial sediment load	5–7 mm/y	Gardner and Jones (1993)

evidence for the existence of such faults, it can be argued that the observed cooling was driven by erosion by surface processes.

Dynamic equilibrium and erosion rates

Definitions

In one of its early definitions, dynamic equilibrium referred to a characteristic that fluctuates around a mean that is itself gradually changing and usually is decreasing (Hack, 1960, 1975). More recently, dynamic equilibrium has been defined in terms of a steady state in which, despite short-term fluctuations, the long-term mean remains unchanged. Dynamic equilibrium in convergent orogens indicates a time-invariant state with respect to some characteristic. For example, an orogen could attain a thermal steady state in which isotherms become fixed with respect to some reference frame, a potential energy steady state in which the mean elevation of the range is invariant, a topographic steady state in which topographic characteristics remain statistically constant through time, or an erosional steady state in which rock uplift and erosion are in balance. In the absence of tectonic extension, topographic and erosional steady states are clearly

closely linked, because the existence of one usually requires the existence of the other.

A topographic steady state has several attributes that must co-exist: both the mean elevation and the topographic relief should be constant. If either of these is changing (Fig. 9), then the topography of the range cannot be in steady state. Whereas it is simple to specify these criteria for steady state, it is difficult to document their validity with respect to any given mountain range. Both mean elevation and relief represent averages across a range. While this relaxes any expectation that any specific position in a landscape would remain unchanged through time, numerous determinations of altitude or relief would be necessary within a given mountain range in order to calculate a meaningful average value for the past. Determinations of palaeoaltitudes are far from certain and can only be undertaken when appropriate data are available (Forest *et al.*, 1999; Gregory, 1994; Sahagian and Maus, 1994; Wolfe *et al.*, 1997). Developing numerous such analyses commonly becomes a daunting and often intractable task. The magnitude of palaeorelief is generally even more difficult to quantify, although studies assessing the impact of topography both on climate (Kutzbach *et al.*, 1993) and on

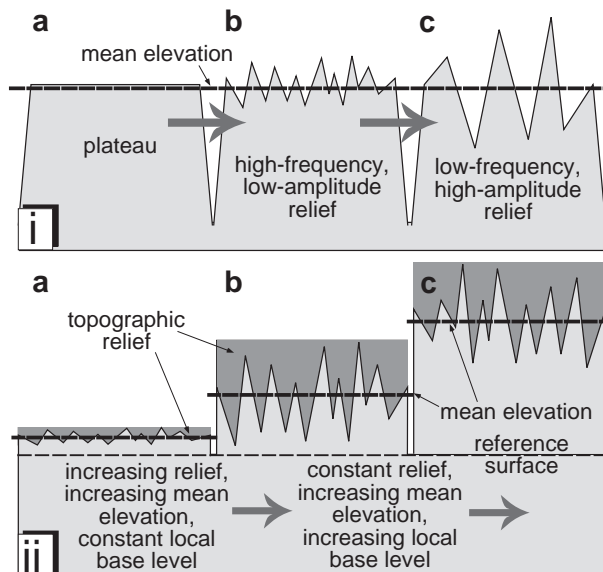


FIG. 9. Both mean relief and elevation should remain constant in a topographic steady state. Changes illustrated here are incompatible with a topographic steady state. (i) Changes in topographic relief with constant mean altitude. (ii) Changes in either relief or mean altitude. Climatically driven changes in relief or mean elevation are expected at time scales of $<10^5$ y, but the mean topography could remain invariant, i.e. steady state, over longer intervals.

RATES OF EROSION AND EXHUMATION

thermochronological ages (Stüwe *et al.*, 1994; House *et al.*, 1998) or using the isotopic fractionation that occurs due to orographic precipitation have shed light on the development of topographic relief in the past (Chamberlain *et al.*, 1999; Chamberlain and Poage, 2000).

The assessment of a topographic steady state should be conducted within an appropriate time frame. Well known Late Cenozoic climate fluctuations (Martinson *et al.*, 1987) changed rainfall distributions, biotic communities, and surface temperatures. Because such changes are expected to influence rates of erosion, it might be expected that erosionally driven topographic changes would occur at common climatic frequencies (Kooi and Beaumont, 1996). For example, if all other conditions were equal, an increase in the discharge of a river would be expected to lower its longitudinal gradient and, therefore, to reduce the elevation of catchment divides that are linked (Fig. 1) to its profile (Whipple *et al.*, 1999). A subsequent change back to previous discharge values would tend to restore the river to its previous gradient. Thus, the topography would be expected to vary at time-scales less than a climatic cycle ($\sim 10^5$ y), but it could be in a dynamic equilibrium when averaged over one or more climate cycles.

Evidence for the existence of dynamic equilibrium

Why should one expect that dynamic equilibrium would exist in collisional ranges? Numerical models that couple geodynamic and surface processes predict that, when tectonic forcing is sufficiently rapid, collisional orogens should attain a dynamic equilibrium (Kooi and Beaumont, 1996; Willett, 1999). This prediction is significant, because it implies that erosion by surface processes will balance rock uplift and advection and, therefore, that rates of unloading recorded by metamorphic rocks (Table 1) can be modulated by rates of erosion. Beyond the predictions of numerical models, a rationale for the existence of topographic steady state derives from the finite strength of crustal rocks and the rates of tectonic processes. Consider the situation in which convergence occurs at 20 mm/y between two continental blocks and drives rock uplift at 10 mm/y within an orogenic transect. In the absence of erosion, elevations within the transect could increase by 10 km/m.y! Within a million years, the strength of crustal rocks would probably be exceeded, and the elevation would

stabilize, either due to extensional faulting in the upper crust or ductile flow in the lower crust. If erosion is permitted to occur, such high mountains would also have high topographic relief along river gorges. This relief would promote landsliding and would serve to regulate maximum elevations. The effects of a relatively small mismatch between the rock uplift and erosion rates lead to similar conclusions. If, for example, the rate at which erosion or extensional processes served to thin the crust were only 10–20% less than the rate of crustal thickening, the mean elevation would increase. After a few million years, this would create the same topographic instabilities as occur in a million years in the absence of erosion or extension.

It is illuminating to consider the implications of the absence of dynamic equilibrium on geomorphic elements in the landscape. For example, a longitudinal river profile approximately connects ridge crests to adjacent basins or sea-level. In the context of the rates posited above (10 mm/y of rock uplift), if uplift were as little as 10% greater than river incision, the elevation of the river profile would increase by 1 km/m.y. Such rates of change in the gradient could not be sustained over long intervals: the steepened gradient would lead to increased shear stress on the bed and would increase the erosion rate of the river. This negative feedback tends to drive a river profile toward an equilibrium configuration, such that river width is adjusted to provide the bed shear stress necessary to erode at a rate that balances rock uplift.

Because of the difficulties, described above, in obtaining data to define a topographic steady state based on mean elevation and relief, commonly other approaches must be used to indicate the presence of dynamic equilibrium within a landscape. One approach consists of a comparison of the spatial distribution of direct or indirect measures of erosion at distinctly different time-scales (Fig. 10). For example, if regional patterns of cooling rates defined through radiometric dating were to display spatial contrasts that were mimicked by patterns of erosion rates derived from studies of fluvial incision or landsliding (Hovius *et al.*, 1997), then it could be argued that these data were supportive of long-term steadiness in the landscape with respect to erosion. In such a case, one would be comparing data at million-year time scales (cooling ages) with data at the decadal to 10^4 -year time-scale (surface process rates). Erosion that is sustained over long

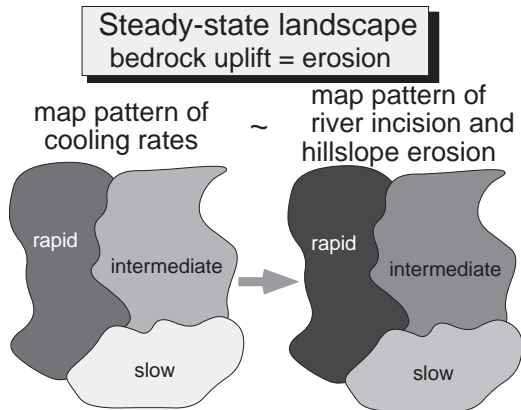


FIG. 10. Spatial patterns of bedrock cooling rates from radiometric dating mimic spatial patterns of erosion based on river incision and hillslope erosion rates. The equivalence implies regional contrasts in erosion have been sustained for protracted intervals. A steady state can be inferred, though not demonstrated, by patterns such as these.

time-spans does not require a steady state, because the landscape could be changing its mean elevation. If it can further be argued, however, that tectonic forcing has been steady over this same interval and, in particular, that the rate of rock uplift has been rapid (greater than a few mm/y), then, based on the geomorphic and geodynamic arguments above, it is likely that the landscape has achieved or is approaching a steady state.

Consider, for example, the northwestern Himalaya in the vicinity of Nanga Parbat (Fig. 11). This is an area where rapid rates and distinct spatial contrasts of bedrock cooling have been documented through numerous radiometric studies (Searle, 1996; Winslow *et al.*, 1996; Zeitler, 1985). Apatite fission-track age (annealing temperature $\sim 120^{\circ}\text{C}$ for rapid cooling) have been particularly useful in delineating recent cooling histories. An elongate, north-south region of rapid cooling coincides with the Nanga Parbat-Haramosh axis (NPHA). Within this zone, apatite fission-track ages are <1 m.y. and indicate cooling rates as rapid as $\sim 350^{\circ}\text{C}/\text{m.y.}$ (Winslow *et al.*, 1996). Fission-track ages become systematically older toward the east and west (Fig. 11), indicating slower cooling rates. A widely distributed suite of biotite $^{40}\text{Ar}/^{39}\text{Ar}$ cooling ages (closure temperature $\sim 300^{\circ}\text{C}$) across the Nanga Parbat region mimics that

pattern of the fission-track ages and delineates a northward-plunging antiformal structure displaying dates as young as 1 m.y. in its core (Winslow *et al.*, 1996). Whereas the geothermal gradient is not well established for this region, reasonable limits on the gradient (Burbank *et al.*, 1996; Craw *et al.*, 1994) suggest that this range of cooling ages corresponds with erosion rates of 1–10 mm/y with the highest rates centred along the NPHA massifs (Fig. 5). Thus, these chronological data provide a long-term (>1 m.y.) record of the regional patterns of erosion.

This long-term pattern can then be compared with the pattern of erosion that is derived from the study of strath terraces in the vicinity of Nanga Parbat that were formed and abandoned during the past 70 ky (Fig. 5). Although the correlation is imperfect and rates of long-term erosion are loosely defined due to an uncertain geotherm, the pattern of spatial variations in erosion rates is remarkably consistent at time-scales ranging from 10^4 to 10^6 years. This correlation underpins, therefore, the interpretation of steady-state erosion through this region at million-year time-scales. Interestingly, although only a few studies of glacial erosion rates have been conducted in this area, modern erosion rates for the Raikot glacier on the flanks of Nanga Parbat are calculated to be 5–7 mm/y (Gardner and Jones, 1993): a rate that is analogous with the river incision rates and is consistent with the long-term rates.

Although spatially varying rates of erosion may be in steady state, a topographic steady state may not exist if the mean elevation or relief is changing. As argued above, if tectonic rates are rapid, collisional orogens should approach a topographic steady state. In the Nanga Parbat region, tectonic forcing is not known to vary significantly during Quaternary times. Range-parallel displacements that are approximately orthogonal to the Raikot Fault (Fig. 11) are estimated to be ~ 12 mm/y (Seeber and Pêcher, 1998). These rates should, in turn, drive rock uplift of >5 mm/y above an east-dipping crustal ramp associated with the Raikot Fault (Butler *et al.*, 1997; Koons, 1998). The combination of rapid erosion and rock uplift rates suggests that the Nanga Parbat region should be in or approaching a dynamic equilibrium.

Implications for landscapes

If a dynamic equilibrium exists and results from erosion that balances rock uplift, how is this

RATES OF EROSION AND EXHUMATION

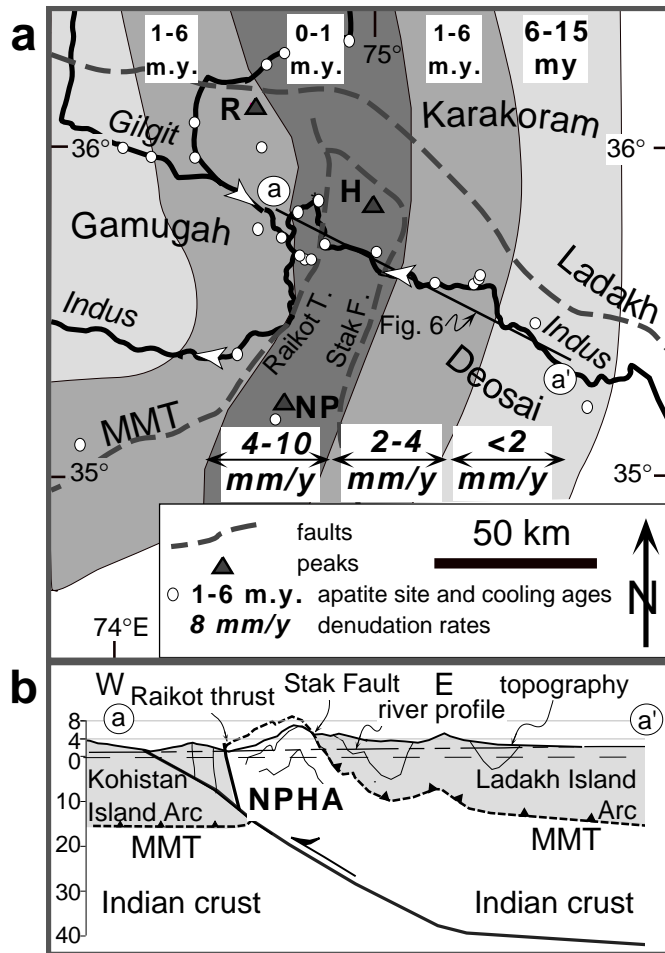


FIG. 11. (a) Map of apatite fission-track cooling ages and inferred rock-uplift rates in the vicinity of Nanga Parbat, northwest Himalaya. The Raikot Fault is an active thrust fault bounding the west flank of the Nanga Parbat-Haramosh axis: a zone of rapid rock uplift inferred from cooling rates. The Stak Fault bounds the eastern margin of the uplift. Fission-track data are from Zeitler (1985). H: Haramosh; MMT: Main Mantle Thrust; NP: Nanga Parbat; R: Rakaposhi. Modified from Burbank *et al.*, 1996. (b) Schematic structural cross section along the line a—a' above. The Nanga Parbat uplift occurs above a crustal scale west-vergent thrust fault. Rock-uplift rates vary as a function of the curving trajectory of the ramp. MMT: Main Mantle Thrust; NPHA: Nanga Parbat-Haramosh Axis.

achieved? In non-glacial settings, both rivers and hillslopes must be eroding as rapidly as the rock is uplifting. River profiles would remain fixed with respect to an external reference frame. Hillslopes could be envisioned in two possible configurations: slope angles could be proportional to the rock uplift and erosion rate, or slope angles could lie at the threshold for landsliding (Fig. 12). In the former case, sediment fluxes off of hillslopes would be dependent on the slope angle, whereas

in the latter case, fluxes would be dependent on the rate of lowering of base level at the toe of the slope (Fig. 12). In the latter case, slopes are considered to be at threshold angles: in other words, at the critical angle for failure by bedrock landslides. These slopes can not steepen significantly, even if the river-incision or rock-uplift rate increases. Instead, they would be predicted to fail more often or in larger slides that would increase the net flux. This model would, therefore, predict

D.W. BURBANK

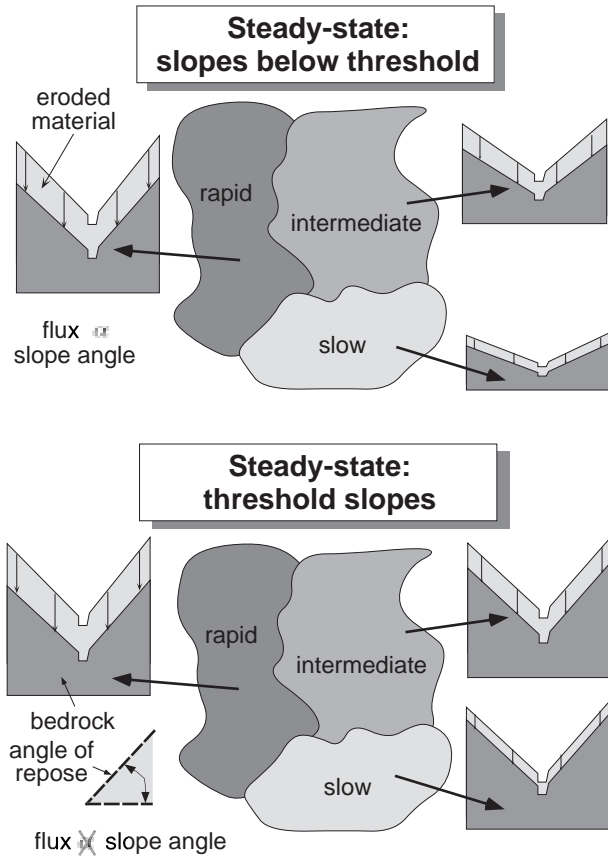


FIG. 12. Models for hillslope erosion rates. Top: flux from hillslopes is proportional to hillslope angle. Bottom: Flux is independent of hillslope angle, because all hillslopes are at threshold slope angles. Hillslope fluxes are controlled by the rate of river erosion and base level lowering.

a predominance of threshold slopes in a rapidly eroding landscape.

With reference again to the northwestern Himalaya (Fig. 11), the distribution of hillslope angles as a function of rock uplift and erosion rate can be assessed using digital topographic data. If slope angles were proportional to erosion rates, there would be a correlation of the mean hillslope angles with the cooling rates shown by the fission-track dating. Based on a 90-m DEM, slope angles were calculated as the best-fit plane to a moving window representing a 4×4 matrix of elevation data. The results reveal a similarity in slope distributions (Burbank *et al.*, 1996) throughout the region (Fig. 13). Despite an order of magnitude difference in erosion rates across the study area (Fig. 5), the histograms of slope angles are nearly indistinguishable among the different subregions.

In fact, the mean slope angle from the Nanga Parbat area, which has the highest erosion rate (Zeitler, 1985), is lower than that for many of the other areas (Fig. 13). All of the subregions that are not part of present plateaux display mean slope angles that are $\sim 31-33^\circ$. This is the angle of repose for many cohesionless materials. The key conclusion to be drawn from these data is that slope distributions are independent of erosion rate. Furthermore, the steep mean-slope angle implies that these slopes are in a threshold condition, such that they cannot be steepened further. In such a case, the flux off of hillslopes and the rate of erosion will be regulated by the rate of local base-level lowering at the toes of the slopes. Given that, even in the less rapidly eroding areas, the mean slopes are $>30^\circ$, another important inference is that, if the long-term

RATES OF EROSION AND EXHUMATION

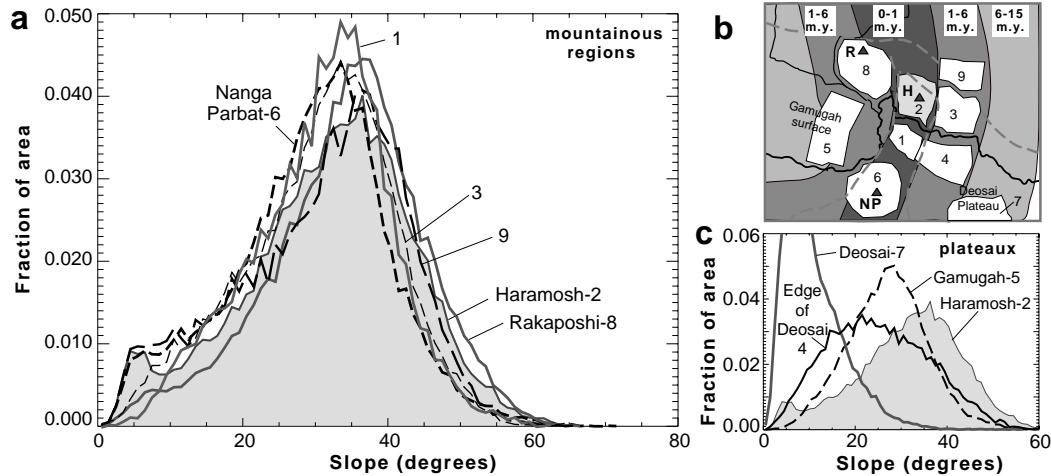


FIG. 13. Slope distributions in the northwest Himalaya in the vicinity of Nanga Parbat. (a) Histograms of slopes for subregions that correspond to high, intermediate, and low erosion rates. No significant difference exists among these histograms. Note that the mean slope angle is $\sim 30^\circ$; equivalent to the angle of repose in many cohesionless materials. (b) Locations of the areas used in slope analysis. Compare this map with Fig. 11 to see the correspondence between selected areas and erosion/cooling rates. H: Haramosh; NP: Nanga Parbat; R: Rakaposhi. The area including Haramosh is shaded as a reference histogram in the other plots. (c) Slope histograms for plateau-like areas near Nanga Parbat. Slopes on a plateau such as Deosai are gentle, and become steeper near the dissected margin of the plateau. The shaded histogram is from Haramosh for reference.

erosion rate is above some threshold value (~ 0.5 mm/y), hillslopes will be poised near the critical angle for failure by bedrock landsliding.

Non-glaciated ranges

When the river incision and hillslope data are considered together, they yield a simple model of dynamic equilibrium when erosion is occurring in a region of rapid deformation (Fig. 14). River incision counterbalances rock uplift rates, such that rocks move upward toward or through a fixed longitudinal river profile. Adjacent hillslopes are maintained near the threshold for failure by bedrock landslides. Unless the spacing between drainages increases over time, any mismatch due to less rapid landsliding in comparison to rock uplift will cause continued steepening of slopes and will eventually lead to slope collapse. These hillslopes will, therefore, fluctuate around a mean angle that represents the upper limit of hillslope strength.

Ranges with warm-based glaciers

Glacial processes yield a more complicated landscape than a non-glacial one. In a dynamic equilibrium, the same combination as described

above of river incision and landsliding operates below the glacial zone. In the topographic region below the glaciers, local base level will still be set by rivers, whereas it will be controlled by glaciers within the glaciated region. Glacial erosion typically smoothes landscapes and decreases mean slope angles, particularly in the altitude range encompassing past and present snowlines (Brozovic *et al.*, 1997). If the drainage spacing does not change between glacial and nonglacial landscapes in the same orogen, then the lowered slope angles resulting from glaciation will cause a decrease in the mean elevation (Fig. 15). Warm-based glaciers (at the pressure-melting point) yield the rapid erosion rates described previously (Fig. 8) and are responsible for planing off the mountains near the snowline (Brozovic *et al.*, 1997; Isacks *et al.*, 1994).

Ranges with cold-based glaciers

Some orogens at high latitudes or with peaks at high altitudes experience sufficiently cold temperatures that glaciers on them are 'cold-based' and are frozen to their beds. This creates an additional 'process zone' where different mechanisms control erosion during dynamic

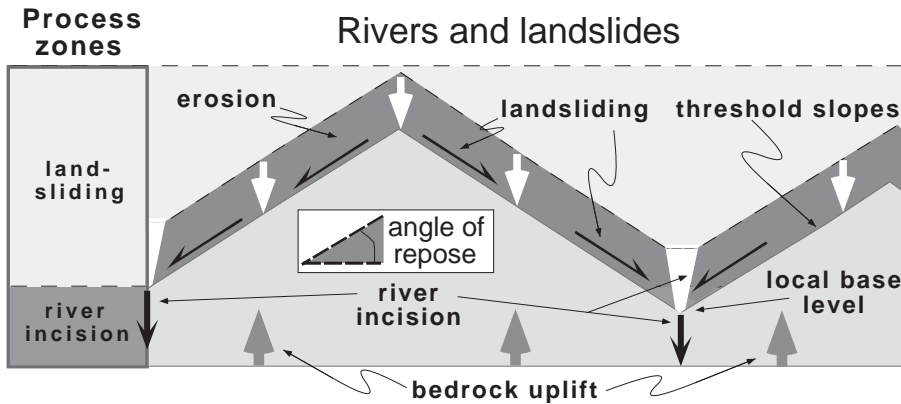


FIG. 14. Process model of dynamic equilibrium for rivers and hillslopes in non-glaciated regions of rapid deformation. Topographic steady state prevails as rates of landsliding on threshold slopes deliver rock to the river valleys, which are themselves lowering at the same rate as the hillslopes. These rates balance the rock uplift rate.

equilibrium (Fig. 16). Cold-based glaciers cause no direct erosion, and in fact, could be viewed as a protective mantle that reduces erosion. On mountains where there is a thermal transition from warm-based glaciers at lower altitudes to cold-based ones on the higher slopes, there is a concomitant change from high to negligible rates of glacial erosion (Fig. 16). The net result is that, as the warm-based glaciers erode headward in the vicinity of the snowline, peaks clad by cold-based glaciers become topographic pedestals with increasing relief and increasingly narrow bases. If rapid rock uplift is occurring, this dictates that the slowly eroding peaks will attain progressively

higher altitudes as the top of the pedestal rises farther above the snowline. Eventually, the resulting topographic tower will exceed the strength of the rock it comprises and will collapse by large-scale rockfalls (Fig. 16). Some late Holocene rockfalls in the Himalaya with volumes exceeding 1 km^3 (Fort, 1987; Yamanaka and Iwata, 1982) appear to have originated from within the cold-based glacier zone ($>6500 \text{ m}$). Without knowing the longer term frequency of such events in a given area, it is difficult to assess their contribution to overall erosion rates. Nonetheless, because peaks will collapse episodically via large rockfalls, the

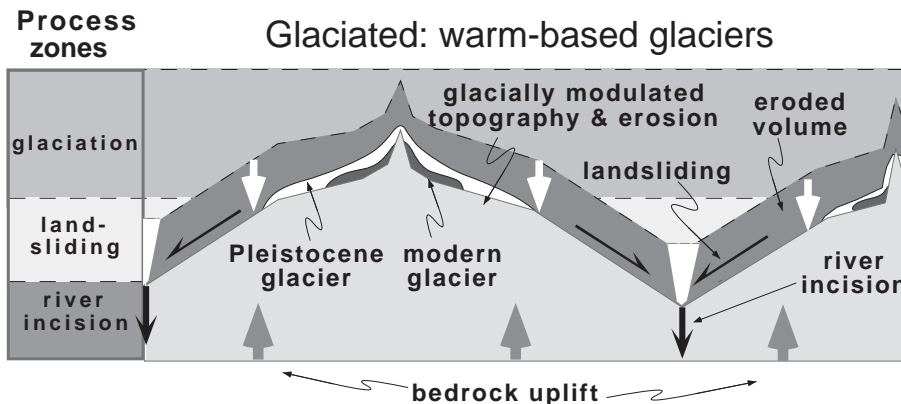


FIG. 15. Process model of dynamic equilibrium for a glaciated landscape. Topography and mean slope angles are lowered in the vicinity of the long-term snowline. Rivers and hillslopes at lower altitudes are behave identically to those shown in Fig. 14.

RATES OF EROSION AND EXHUMATION

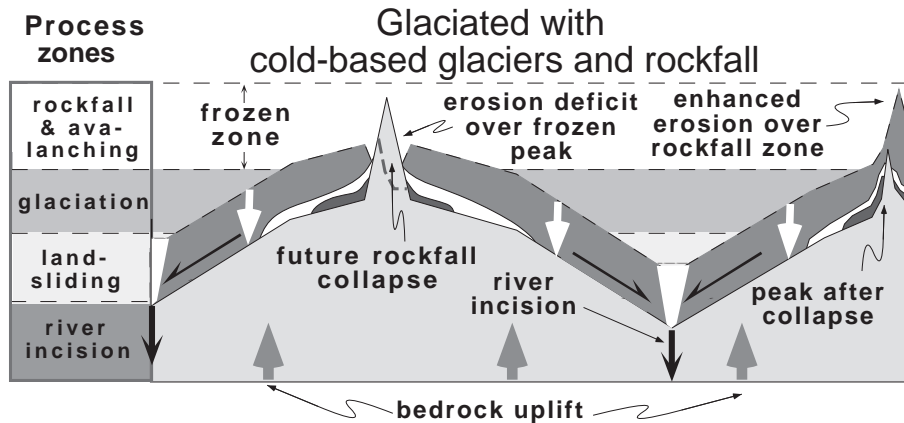


FIG. 16. Process model of dynamic equilibrium for a glaciated landscape with both cold- and warm-based glaciers. Little to no erosion occurs in the zone of cold-based glaciers, so that peak altitudes increase linearly with rock uplift. Erosion by warm-based glaciers creates an increasingly narrow pinnacle of rock beneath the frozen summits. When the strength of the rock is exceeded, infrequent, large-scale rockfalls abruptly reduce the height of the peaks.

maximum topography should display broader fluctuations when cold-based glaciers are present than would prevail in either the non-glacial or warm-based glacial scenarios. On the other hand, the highest 20% of the topographic relief in high mountain ranges commonly represents only 2–3% of the total area (Brozovic *et al.*, 1997). Collapse of summit pedestals, therefore, typically have only a small impact on the mean elevation or mean erosion rates of a range.

Discussion and Synthesis

The process models described above (Figs 14–16) provide a framework for linking diverse topographic elements and erosional mechanisms in a landscape displaying dynamic equilibrium. The quantification of rates of erosion (Table 2) by river incision (Burbank *et al.*, 1996), bedrock landsliding (Hovius *et al.*, 1997), and warm-based glaciers (Hallet *et al.*, 1996) indicates that each of these processes is sufficiently rapid to account for many of the reconstructed rates of unloading or cooling that have been estimated through geobarometry or thermochronology (Table 1). Many of the erosion measurements described here represent calculations at a point in a landscape, for example, at the toe of a glacier or a particular strath terrace. From a skeptical perspective, these rates might be regarded as extreme or rare events that are unlikely to be sustainable for 10^5 to 10^6 y.

The geological context in which at least some of the rates were determined argues against such a contention. For example, although each incision rate calculation along the Indus River is an independent determination (Burbank *et al.*, 1996), the suite of dates along the river (Fig. 5) presents a smoothly varying range of rates that correlates well with cooling ages in the underlying bedrock (Zeitler, 1985). Perhaps such rates are only sustainable during glacial-interglacial transitions, but the spatial variations in rates indicate that rock uplift, rather than climate, is the primary cause of spatial differences. Similarly, the glacial erosion rates on the flanks of Nanga Parbat (Raikot Glacier: Gardner and Jones, 1993) are also nearly equivalent to the long-term erosion rates. The landslide flux calculations in New Zealand represent an integration throughout several large catchments (Hovius *et al.*, 1997). Although the analysis relies on 20th century aerial photographs, anthropogenic influences on landslide initiation are minimal in the study area. Whereas the maximum length scaling (L_1 in equation 5) that is used to calculate the flux might lead to an overestimated rate, the regional pattern of rates is consistent with the rates inferred from fission-track dating and geodynamic models of the Southern Alps (Koons, 1989; Tippett and Kamp, 1995; Willett, 1999). Thus, in both the Himalaya and the Southern Alps, existing geologic and geodynamic data provide a framework in which the simplest way to account for

patterns of regional deformation and exhumation is using the observed surface erosion rates.

Direct comparison of landsliding or river incision rates with thermochronologically estimated rates of denudation from the same range provides the most compelling case for balanced erosion and rock uplift rates. With the exception of the Raikot Glacier on Nanga Parbat, there are few such direct comparisons for glaciated landscapes. One can argue logically, however, that glaciers must be as effective erosional agents as rivers and landslides. In drainages where only the head of the catchment has been extensively glaciated, the glaciated valley gradient is commonly lower than in nearby non-glaciated catchments, thus indicating that the glaciers incised more efficiently than the headwater rivers (Brocklehurst and Whipple, in press). In both the Southern Alps and the Himalaya (Table 2), where documented landslide and fluvial denudation rates account for 10s of km of orogenic denudation, modern glaciation is extensive. Despite the fact that these glaciers are at a minimal, interglacial size at present, they reside in the bottom of large, steep-walled valleys. If glacial erosion was incapable of matching or exceeding the rates of landsliding, rockfall, and river incision, the glaciers should occupy high points in the landscape, rather than valley bottoms. Indeed, the cold-based glaciers, which are not eroding effectively, do occupy the high parts of the landscape, whereas the warm-based glaciers have scoured at least as rapidly as the adjacent rivers. In the Southern Alps, the glaciers extend up to and across the Alpine Fault at altitudes near sea level. Clearly, the glaciers have been able to keep pace with the ~ 10 mm/y rock uplift rate along this fault.

Another perspective on the relative importance of tectonic extension versus erosion in modern collisional orogens derives from seismic and structural studies. Of those orogens experiencing rapid shortening and rock uplift, which of them display structural or seismic evidence for extensional faulting at the shallow crust depths that would be required to explain available fission-track or (U-Th)/He dates? Given that these thermochronometers typically record cooling of rocks at depths of 2–4 km, any normal faulting that caused this cooling would have to occur along brittle structures between the surface and these shallow depths. There are few collisional orogens where active extensional structures with large displacements have been documented at shallow depths.

Consider the intensively studied Nanga Parbat massif which is characterized by rapid cooling ($>150^\circ\text{C}/\text{m.y.}$) during the past 3–5 m.y. Extensional structures have been described to the west of the massif (Hubbard *et al.*, 1995) and have been suggested as structures that accommodated tectonic exhumation. More recent thermochronology, however, indicates that these structures are Miocene or older in age and cannot account for the recent cooling history (Edwards *et al.*, 1996). In fact, the most recent structural studies around Nanga Parbat conclude that the “rapid and young exhumation is not due to orogen-scale structural unroofing” (Schneider *et al.*, 1999). Seismological data collected around Nanga Parbat yield extensional fault-plane solutions at shallow depths within the antiform (Meltzer *et al.*, 1998). These might be interpreted to represent tectonic structures that would accommodate exhumation. Considerable seismicity, however, occurs within the edifice of the Nanga Parbat massif which rises 7 km above local base level. Such seismicity is more consistent with gravitational collapse through massive landsliding than it is with normal faulting, because candidate structures for these normal faults would terminate along the sides of the massif, as would glide planes of landslides, rather than extending downward through the brittle crust.

Even if tectonic extension does cause significant denudation in massifs like Nanga Parbat, the measured rates of river incision require rock uplift and erosion to be nearly in balance. Consider, for example, the implications of hypothetical extensional faulting at Nanga Parbat. The massif itself would be expected to lie in the hangingwall of the normal fault. Rates of river incision would be calculated with respect to material points in this ‘hangingwall’, such that the river bed would be moving downward with respect to the rocks of the hangingwall (Fig. 17). Extensional faulting also causes material points within the hangingwall to move downward with respect to sea-level. Under these circumstances, the altitudinal position of the river bed would represent the additive results of river incision and the hangingwall subsidence. If the combined river incision and subsidence were not nearly balanced by rock uplift, the longitudinal profile of the river would soon attain an unacceptable geometry: it would be lower than sea-level. Today, for example, the Indus River lies ~ 1 km above sea-level as it crosses the Nanga Parbat massif. If the rates of bedrock incision as calibrated over the past 3×10^4 y (Burbank *et al.*,

RATES OF EROSION AND EXHUMATION

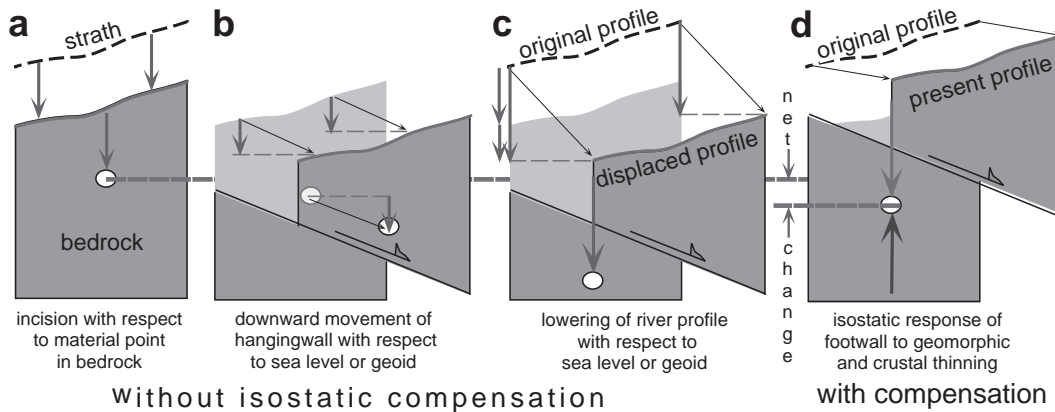


FIG. 17. Changes in the position of the longitudinal profile of a river due to incision and extensional faulting. (a) Strath terraces indicate the amount of lowering of the river profile that has occurred with respect to the bedrock into which it is incising. (b) Normal faulting causes lowering of points within the hangingwall with respect to sea level or the geoid. (c) Net change in the river profile without isostatic compensation is the sum of the incision into the bedrock plus any change in the height of the hangingwall. (d) With isostatic compensation, ~80% of the change in profile height will be restored by footwall uplift.

1996) were sustained for $1-2 \times 10^5$ y, parts of the river profile would end up below sea-level. This obviously cannot occur: if extension is occurring, it must be overwhelmed in the shallow crust by shortening and rock uplift. The only circumstances in which such incision rates could exist in the absence of significant rock uplift would be if the river system were in a transitory condition caused by a switch to a more erosive state (Whipple *et al.*, 1999). This cannot be the primary driving force for fluvial downcutting at Nanga Parbat because it is inconsistent with the spatial distribution of incision rates (Fig. 5).

Despite the potentially rapid rates of erosion by surface processes (Table 2), the role of extension in crustal thinning in collisional orogens can not be dismissed. So far, no long-term rates of geomorphic denudation have been shown to be sufficient to balance completely the rates of thinning documented for some ultrahigh- P terranes (Table 1). The unloading rates of 20–40 mm/y are considerably more rapid than documented geomorphic rates, with the possible exception of glacial erosion (Table 2). The examples of rapid unloading of ultrahigh- P rocks involve upward transit of previously subducted crustal rocks through the mantle. We have little knowledge of the mechanisms by which the lithosphere accommodates this vertical advection, which could

potentially occur without significant erosion or extension in the brittle crust.

Nonetheless, there is clear evidence for extension in collisional orogens in the past (Balanya *et al.*, 1997; Burchfiel *et al.*, 1992; Flinch, 1996; Platt, 1986). Several types of geological evidence could be used to suggest extensional collapse in modern collisional belts, e.g. the presence of normal faults and other structural indicators of extension at shallow depths, shallow seismicity with normal-fault solutions, and juxtaposition of low-grade or unmetamorphosed rocks over high-grade rocks support tectonic exhumation. Consider the situation in which plate tectonic movements or geodetic data indicate that two continental blocks are colliding at high rates. If, despite this rapid convergence, young cooling ages or evidence for rapid geomorphic erosion at the surface are largely absent, then it is likely that extensional collapse of the orogen is depressing rates of erosion or that underthrusting without significant crustal thickening is occurring. Because extensional thinning is spatially restricted to rocks above the normal fault itself, however, it is commonly impossible for such tectonic denudation to account for orogen-wide erosion. Some combination of tectonic and geomorphic erosion must cause any observed crustal thinning.

In order to address the relationship of erosion and exhumation more fully, interdisciplinary studies that are focused on orogenic transects are needed. Coordinated studies that merge geochronology, geobarometry, geodesy, geomorphology, seismology and structure have the potential to provide an integrated assessment of the interactions among competing processes in the growth and erosion of orogens. Recent studies provide a clear indication that surface processes are capable of eroding at rates exceeding 5 km/m.y. Rather than attributing most intervals of rapid unloading to extensional faulting, the documentation of rapid geomorphic erosion rates prompts a different suite of questions concerning extension in collisional orogens. For example, what combination of changes in tectonic and geomorphic rates or climatic and lithologic controls cause rock uplift to outpace erosion, so that extensional collapse occurs? More specifically, in the Himalaya, the quintessential collisional range, one might ask what conditions prevailed at 15–20 Ma, such that erosion was unable to keep pace with rock uplift, and instead a system of normal faults spanning the length of the Himalaya became active? The answers to these questions will further illuminate the interactions between surface and tectonic processes in modulating exhumation.

Acknowledgements

This research was supported by grants from NSF (EAR 922056; 9627865, 9896048, 9909647) and NASA (NAGW-3762; NAG5-7646; -7781). The ideas in this paper were motivated through discussions with Andrew Meigs, Bob Anderson, Nick Brozovic, Jérôme Lavé, Ian Brewer, Niels Hovius, Eric Kirby, Jaume Vergès, Eric Fielding and Kip Hodges to whom I am grateful. Ann Blythe kindly provided two fission-track analyses which are depicted in Fig. 6. Jaume Vergès created the original cross-section in Fig. 11. Thoughtful reviews by Hugh Sinclair and Brian Bluck significantly improved this manuscript.

References

- Allen, P.A. (1997) *Earth Surface Processes*. Blackwell Science, Oxford, UK.
- Amato, J.M., Johnson, C.M., Baumgartner, L.P. and Beard, B.L. (1999) Rapid exhumation of the Zermatt-Saas ophiolite deduced from high-precision Sm–Nd and Rb–Sr geochronology. *Earth and Planetary Science Letters*, **171**, 425–438.
- Anderson, R.S. (1994) Evolution of the Santa Cruz Mountains, California, through tectonic growth and geomorphic decay. *Journal of Geophysical Research*, **99**, 20,161–20,179.
- Anderson, R.S. and MacGregor, K.C. (1998) The role of glacial erosion in mountain range evolution. *EOS (Transactions of the American Geophysical Union)*, **79**, 337.
- Andrews, D.J. and Hanks, T.C. (1985) Scarps degraded by linear diffusion: inverse solution for age. *Journal of Geophysical Research*, **90**, 10193–10208.
- Balanyà, J.C., García-Dueñas, V., Azañón, J.M. and Sánchez-Gómez, M. (1997) Alternating contractional and extensional events in the Alpujarride nappes of the Alborán Domain (Betics, Gibraltar Arc). *Tectonics*, **16**, 226–238.
- Beaumont, C., Fullsack, P. and Hamilton, J. (1992) Erosional control of active compressional orogens. Pp. 1–18 in: *Thrust Tectonics* (K.R. McClay, editor). Chapman & Hall, London.
- Bierman, P. (1994) Using in situ produced cosmogenic isotopes to estimate rates of landscape evolution: a review from the geomorphic perspective. *Journal of Geophysical Research*, **99**, 13,885–13,896.
- Brandon, M.T., Roden-Tice, M.K. and Garver, J.I. (1998) Late Cenozoic exhumation of the Cascadia accretionary wedge in the Olympic Mountains, northwest Washington State. *Geological Society of America Bulletin*, **110**, 985–1009.
- Brocklehurst, S.H. and Whipple, K.X. (2002) Glacial erosion and relief production in the eastern Sierra Nevada, California. *Geomorphology* (in press).
- Brozovic, N., Burbank, D.W. and Meigs, A.J. (1997) Climatic limits on landscape development in the northwestern Himalaya. *Science*, **276**, 571–574.
- Bull, W.B. (1991) *Geomorphic Responses to Climatic Change*. Oxford University Press, London.
- Bull, W.B. and Cooper, A.F. (1986) Uplifted marine terraces along the Alpine fault, New Zealand. *Science*, **234**, 1225–1228.
- Burbank, D.W., Leland, J., Fielding, E., Anderson, R.S., Brozovic, N., Reid, M.R. and Duncan, C. (1996) Bedrock incision, rock uplift and threshold hillslopes in the northwestern Himalaya. *Nature*, **379**, 505–510.
- Burbank, D.W., Lavé, J., Meigs, A.J., Fielding, E.F. and Blythe, A.E. (1998) Consistent long and short-term denudation patterns in the San Gabriel and Himalayan Mountains. *EOS (Transactions of the American Geophysical Union)*, **79**, 338.
- Burchfiel, B.D., Zhileng, C., Hodges, K.V., Yuping, L., Royden, L.H., Changrong, D. and Jiene, X. (1992) *The South Tibetan Detachment System, Himalayan Orogen: Extension Contemporaneous with and*

RATES OF EROSION AND EXHUMATION

- Parallel to Shortening in a Collisional Mountain Belt*. Geological Society of America, Special Paper **269**.
- Butler, R.W.H., Harris, N.B.W. and Whittington, A.G. (1997) Interactions between deformation, magmatism and hydrothermal activity during active crustal thickening: a field example from Nanga Parbat, Pakistan Himalayas. *Mineralogical Magazine*, **61**, 37–52.
- Chamberlain, C.P. and Poage, M.A. (2000) Reconstructing the paleotopography of mountain belts from the isotopic composition of authigenic minerals. *Geology*, **28**, 115–118.
- Chamberlain, C.P., Poage, M.A., Craw, D. and Reynolds, R.C. (1999) Topographic development of the Southern Alps recorded by the isotopic composition of authigenic clay minerals, South Island, New Zealand. *Chemical Geology*, **155**, 279–294.
- Church, M. and Slaymaker, O. (1989) Disequilibrium of Holocene sediment yield in glaciated British Columbia. *Nature*, **337**, 452–454.
- Clark, D.H., Clark, M.M. and Gillespie, A.R. (1994) Debris-covered glaciers in the Sierra Nevada, California and their implications for snowline reconstructions. *Quaternary Research*, **41**, 139–153.
- Craw, D., Koons, P.O., Winslow, D., Chamberlain, C.P. and Zeitler, P. (1994) Boiling fluids in a region of rapid uplift, Nanga Parbat massif, Pakistan. *Earth and Planetary Science Letters*, **128**, 169–182.
- Edwards, M.A., Kidd, W.S.F., Seeber, L., Pecher, A., LeFort, P., Riaz, R. and Khan, M.A. (1996) An upwardly mobile indenter? The Nanga Parbat-Haramosh massif viewed as a crustal scale pop-up structure. *EOS (Transactions of the American Geophysical Union)*, **77**, 692.
- Fitzgerald, P.G., Sorkhabi, R.B., Redfield, T.F. and Stump, E. (1995) Uplift and denudation of the central Alaska Range: a case study in the use of apatite fission track thermochronology to determine absolute uplift parameters. *Journal of Geophysical Research*, **100**, 20,175–20,191.
- Flinch, J.F. (1996) Accretion and extensional collapse of the external Western Rif (Northern Morocco). Pp. 61–85. in: *Peri-Tethys Memoir 2: Structure and Prospects of Alpine Basins and Forelands*. (P.A. Ziegler and F. Horváth, editors). Mémoires du Muséum National d'Histoire Naturelle, **170**, Paris.
- Forest, C.E., Wolfe, J.A., Molnar, P. and Emanuel, K.A. (1999) Palealtimetry incorporating atmospheric physics and botanical estimates of paleoclimate. *Geological Society of America Bulletin*, **111**, 1497–511.
- Fort, M. (1987) Sporadic morphogenesis in a continental subduction setting: an example from the Annapurna Range, Nepal Himalaya. *Zeitschrift für Geomorphologie*, **63**, 9–36.
- Foster, D.A., Gleadow, A.J.W. and Mortiner, G. (1994) Rapid Pliocene exhumation in the Karakoram (Pakistan), revealed by fission-track thermochronology of the K2 gneiss. *Geology*, **22**, 19–22.
- Foster, D.A. and John, B.E. (1999) Quantifying tectonic exhumation in an extensional orogen with thermochronology: examples from the southern Basin and Range Province. Pp. 343–364 in: *Exhumation Processes: Normal Faulting, Ductile Flow and Erosion* (U. Ring, M.Y. Brandon, G.S. Lister and S.D. Willett, editors). Special Publication **154**, Geological Society, London.
- Galy, A. and France-Lanord, C. (2001) Higher erosion rates in the Himalaya: Geochemical constraints on riverine fluxes. *Geology*, **29**, 23–26.
- Gardner, J.S. and Jones, N.K. (1993) Sediment transport and yield at the Raikot Glacier, Nanga Parbat, Punjab Pakistan. Pp. 184–197 in: *Himalaya to the Sea: Geology, Geomorphology and the Quaternary* (J.F. Shroder Jr., editor). Routledge, London.
- Gregory, K. (1994) Palaeoclimate and palaeoelevation of the 35 Ma Florrisant flora, Front Range, Colorado. *Palaeoclimatology*, **1**, 23–57.
- Guillot, S., Cosca, M., Allemand, P. and Le Fort, P. (1999) Contrasting metamorphic and geochronologic evolution along the Himalayan belt. *Geological Society of America Special Paper*, **328**, 117–128.
- Hack, J.T. (1960) Interpretation of erosional topography in humid temperate regions. *American Journal of Science*, **258-A**, 80–97.
- Hack, J.T. (1975) Dynamic equilibrium and landscape evolution. Pp. 87–102 in: *Theories of Landform Evolution* (W.N. Melhorn and R.C. Flemal, editors). Allen and Unwin, Boston, USA.
- Hacker, B.R., Calvert, A., Zhang, R.Y., Ernst, G.W. and Liou, J.G. (in review) Ultra-Rapid Exhumation of Ultrahigh-Pressure Diamond-Bearing Metasedimentary Rocks of the Kokchetav Massif. *Earth and Planetary Science Letters*.
- Hallet, B. (1979) A theoretical model of glacial abrasion. *Journal of Glaciology*, **23**, 39–50.
- Hallet, B., Hunter, L. and Bogen, J. (1996) Rates of erosion and sediment evacuation by glaciers: a review of field data and their implications. *Global Planetary Change*, **12**, 213–235.
- Hanks, T.C., Bucknam, R.C., LaJoie, K.R. and Wallace, R.E. (1984) Modification of wave-cut and faulting controlled landforms. *Journal of Geophysical Research*, **89**, 5771–5790.
- Harbor, J.M., Hallet, B. and Raymond, C.F. (1988) A numerical model of landform development by glacial erosion. *Nature*, **333**, 347–349.
- Harrison, T.M., Ryerson, F.J., Le Fort, P., Yin, A., Lovera, O.M. and Catlos, E.J. (1997) A late Miocene-Pliocene origin for the central Himalayan

- inverted metamorphism. *Earth and Planetary Science Letters*, **146**, E1–E7.
- Heimsath, A.M. (1999) *The Soil Production Function*. PhD thesis, University of California, Berkeley.
- Heimsath, A.M., Dietrich, W.E., Nishiizumi, K. and Finkel, R.C. (1997) The soil production function and landscape equilibrium. *Nature*, **388**, 358–361.
- Heimsath, A.M., Dietrich, W.E., Nishiizumi, K. and Finkel, R.C. (1999) Cosmogenic nuclides, topography and the spatial variation of soil depth. *Geomorphology*, **27**, 151–172.
- Horton, R.E. (1945) Erosional development of streams and their drainage basins, hydrophysical approach to quantitative morphology. *Geological Society of America Bulletin*, **56**, 275–370.
- House, M.A., Wernicke, B.P. and Farley, K.A. (1998) Dating topography of the Sierra Nevada, California, using apatite (U-Th)/He ages. *Nature (London)*, **396**(6706), 66–69.
- Hovius, N., Stark, C.P. and Allen, P.A. (1997) Sediment flux from a mountain belt derived by landslide mapping. *Geology*, **25**, 231–234.
- Hovius, N., Stark, C.P., Chu, H.T. and J.-C.L. (2000) Supply and removal of sediment in a landslide-dominated mountain belt: Central Range, Taiwan. *Journal of Geology*, **108**, 73–90.
- Howard, A.D., Dietrich, W.E. and Seidl, M.A. (1994) Modeling fluvial erosion on regional to continental scales. *Journal of Geophysical Research*, **99**, 13,971–13,986.
- Hubbard, M.S., Spencer, D.A. and West, D.P. (1995) Tectonic exhumation of the Nanga Parbat massif, northern Pakistan. *Earth and Planetary Science Letters*, **133**, 213–225.
- Humphrey, N.F. and Raymond, C.F. (1994) Hydrology, erosion and sediment production in a surging glacier: The Variegated Glacier surge, 1982–1983. *Journal of Glaciology*, **40**, 539–552.
- Isacks, B., Masek, J., Fielding, E., Jordan, T., Bloom, A., Cook, K. and Anonymous (1994) Tectonic/climatic erosion machines. *Geological Society of America Abstracts with Program*, **26**, 382–383.
- Kamp, P.J.J. and Tippett, J.M. (1993) Dynamics of Pacific plate crust in the South Island (New Zealand) zone of oblique continent-continent convergence. *Journal of Geophysical Research*, **98**, 16,107–16,118.
- Kooi, H. and Beaumont, C. (1996) Large-scale geomorphology: classical concepts reconciled and integrated with contemporary ideas via a surface processes model. *Journal of Geophysical Research*, **101**, 3361–3386.
- Koons, P.O. (1989) The topographic evolution of collisional mountain belts: A numerical look at the Southern Alps, New Zealand. *American Journal of Science*, 1041–1069.
- Koons, P.O. (1998) Big mountains, big rivers, and hot rocks. *EOS (Transactions of the American Geophysical Union)*, **79**, 908.
- Kutzbach, J.E., Prell, W.L. and Ruddiman, W.F. (1993) Sensitivity of Eurasian climate to surface uplift of the Tibetan Plateau. *Journal of Geology*, **100**, 177–190.
- Lavé, J. and Avouac, J. P. (2000) Active folding of fluvial terraces across the Siwalik Hills, Himalaya of central Nepal. *Journal of Geophysical Research*, **105**, 5735–5770.
- Leland, J., Reid, M.R., Burbank, D.W., Finkel, R. and Caffee, M. (1998) Late Pleistocene history of bedrock incision and differential uplift along the Indus River near Nanga Parbat, Pakistan Himalaya, from ^{10}Be and ^{26}Al exposure age dating of bedrock straths. *Earth and Planetary Science Letters*, **54**, 93–105.
- MacGregor, K.C., Anderson, R.S., Anderson, S.P. and Waddington, E.D. (1998) Glacially driven evolution of long valley profiles and implications for alpine landscape evolution. *EOS (Transactions of the American Geophysical Union)*, **79**, 337.
- Martinson, D.G., Pisias, N.G., Hays, J.D., Imbrie, J., Moore, T.C. and Shackleton, N.J. (1987) Age dating and orbital theory of the ice ages: Development of a high resolution 0 to 300,000-year chronostratigraphy. *Quaternary Research*, **27**, 1–29.
- Meigs, A. (1998) Bedrock landsliding forced by deglaciation: Three possible examples from the Chugach/St. Elias Range, Alaska. *EOS (Transactions of the American Geophysical Union)*, **79**, 337.
- Meltzer, A., Sarker, G., Seeber, L. and Armbruster, J. (1998) Snap, crackle, pop! Seismicity and crustal structure at Nanga Parbat, Pakistan, Himalaya. *EOS (Transactions of the American Geophysical Union)*, **79**, 909.
- Milliman, J.D. (1997) Fluvial sediment discharge to the sea and the importance of regional tectonics. Pp. 240–258 in: *Tectonic Uplift and Change* (W.F. Ruddiman, editor). Plenum, New York.
- Milliman, J.D. and Syvitski, J.P.M. (1992) Geomorphic/tectonic control of sediment discharge to the ocean: The importance of small mountainous rivers. *Journal of Geology*, **100**, 525–544.
- Montgomery, D.R. and Dietrich, W.E. (1994) A physically based model for the topographic control on shallow landsliding. *Water Resources Research*, **30**, 1153–1171.
- Nishiizumi, K., Kohl, C.P., Arnold, J.R., Dorn, R., Klein, J., Fink, D., Middleton, R. and Lal, D. (1993) Role of *in situ* cosmogenic nuclides ^{10}Be and ^{26}Al in the study of diverse geomorphic processes. *Earth Surface Processes and Landforms*, **18**, 407–425.
- Ohmori, H. (1992) Morphological characteristics of the

RATES OF EROSION AND EXHUMATION

- scar created by large-scale rapid mass movement. *Japanese Geomorphology Union Transactions*, **13**, 185–202.
- Platt, J.P. (1986) Dynamics of orogenic wedges and the uplift of high-pressure metamorphic rocks. *Geological Society of America Bulletin*, **97**, 1037–1053.
- Porter, S.C. (1989) Some geological implication of average Quaternary glacial conditions. *Quaternary Research*, **32**, 245–261.
- Roering, J.J., Kirchner, J.W. and Dietrich, W.E. (1999) Evidence for nonlinear, diffusive sediment transport on hillslopes and implications for landscape morphology. *Water Resources Research*, **35**, 853–870.
- Rosenbloom, N.A. and Anderson, R.S. (1994) Hillslope and channel evolution in a marine terraced landscape, Santa Cruz, California. *Journal of Geophysical Research*, **99**, 14,013–14,029.
- Rubatto, D. and Hermann, J. (2001) Exhumation as fast as subduction? *Geology*, **29**, 3–6.
- Sahagian, D.L. and Maus, J.E. (1994) Basalt vesicularity as a measure of atmospheric pressure and palaeo-elevation. *Nature*, **372**, 449–451.
- Schmidt, K.M. and Montgomery, D.R. (1995) Limits to relief. *Science*, **270**, 617–620.
- Schmidt, K.M. and Montgomery, D.R. (1996) Rock mass strength assessment for bedrock landsliding. *Environmental Engineering Geoscience*, **2**, 325–338.
- Schneider, D.A., Edwards, M.A., Kidd, W.S.F., Asif Khan, M., Seeber, L. and Zeitler, P.K. (1999) Tectonics of Nanga Parbat, western Himalaya; synkinematic plutonism within the doubly vergent shear zones of a crustal-scale pop-up structure. *Geology*, **27**, 999–1002.
- Schumm, S.A., Mosley, M.P. and Weaver, W.E. (1987) *Experimental Fluvial Geomorphology*. 413 pp. John Wiley & Sons, New York.
- Searle, M.P. (1996) Cooling history, erosion, exhumation and kinematics of the Himalaya-Karakoram-Tibet orogenic belt. Pp. 110–137 in: *Asian Tectonics* (A. Yin and M.A. Harrison, editors). Cambridge University Press, Cambridge, UK.
- Seeber, L. and Pêcher, A. (1998) Strain partitioning along the Himalayan arc and the Nanga Parbat antiform. *Geology*, **26**, 791–794.
- Seidl, M.A., Dietrich, W.E. and Kirchner, J.W. (1994) Longitudinal profile development into bedrock: an analysis of Hawaiian channels. *Journal of Geology*, **102**, 457–474.
- Selby, M.J. (1982) Controls on the stability and inclination of hillslopes on hard rock. *Earth Surface Processes and Landforms*, **7**, 449–467.
- Sklar, L. and Dietrich, W.E. (1998) River longitudinal profiles and bedrock incision models stream power and the influence of sediment supply. Pp. 237–260 in: *River Over Rock: Fluvial Processes in Bedrock Channels* (K.J. Tinkler and E.E. Wohl, editors). American Geophysical Union Geophysical Monograph, **107**, Washington, D.C.
- Slingerland, R. and Snow, R.S. (1988) Stability analysis of a rejuvenated fluvial system. *Zeitschrift für Geomorphologie*, **67**, 93–102.
- Small, E.E., Anderson, R.S., Repka, J.L. and Finkel, R. (1997) Erosion rates of alpine bedrock summit surfaces deduced from in situ ¹⁰Be and ²⁶Al. *Earth and Planetary Science Letters*, **150**, 413–425.
- Stüwe, K., White, L. and Brown, R. (1994) The influence of eroding topography on steady-state isotherms: application to fission track analysis. *Earth and Planetary Science Letters*, **124**, 63–74.
- Thomson, S.N., Stöckhert, B. and Brix, M.R. (1999) Miocene high-pressure metamorphic rocks of Crete, Greece: rapid exhumation by buoyant escape. Pp. 87–107 in: *Exhumation Processes: Normal Faulting, Ductile Flow and Erosion* (U. Ring, M.Y. Brandon, G.S. Lister and S.D. Willett, editors). Special Publication **154**. Geological Society, London.
- Tinkler, K.J. and Wohl, E.E. (1998) *River Over Rock: Fluvial Processes in Bedrock Channels*. American Geophysical Union Geophysical Monograph **107**, Washington, D.C.
- Tippett, J.M. and Kamp, P.J.J. (1993) Fission track analysis of the Late Cenozoic vertical kinematics of continental Pacific crust, South Island, New Zealand. *Journal of Geophysical Research*, **98**, 16,119–16,148.
- Tippett, J.M. and Kamp, P.J.J. (1995) Quantitative relationships between uplift and relief parameters for the Southern Alps, New Zealand, as determined by fission track analysis. *Earth Surface Processes and Landforms*, **20**, 153–175.
- Weiland, R.J. and Cloos, M. (1996) Pliocene-Pleistocene asymmetric unroofing of the Irian fold belt, Irian Jaya, Indonesia: Apatite fission-track thermochronology. *Geological Society of America Bulletin*, **108**, 1438–1449.
- Wernicke, B. (1992) Cenozoic extensional tectonics of the U.S. Cordillera. Pp. 553–581 in: *The Geology of North America G-3* (B.C. Burchfiel, P.W. Lipman and M.L. Zoback, editors). Geological Society of America, Boulder, CO, USA.
- Whipple, K.E., Kirby, E. and Brocklehurst, S.H. (1999) Geomorphic limits to climate-induced increases in topographic relief. *Nature*, **401**, 39–43.
- Willett, S.D. (1999) Orogeny and orography: the effects of erosion on the structure of mountain belts. *Journal of Geophysical Research*, **104**, 28,957–28,982.
- Winslow, D.W., Zeitler, P.K., Chamberlain, C.P. and Williams, I.S. (1996) Geochronologic constraints on

D.W. BURBANK

- syntaxial development in the Nanga Parbat region, Pakistan. *Tectonics*, **15**, 1292–1308.
- Wolf, R.A., Farley, K.A. and Kass, D.M. (1998) Modeling of the temperature sensitivity of the apatite (U-Th)/He thermochronometer. *Chemical Geology*, **148**, 105–114.
- Wolfe, J.A., Schorn, H.E., Forest, C.E. and Molnar, P. (1997) Paleobotanical evidence for high altitudes in Nevada during the Miocene. *Science*, **276**, 1672–1675.
- Yamanaka, H. and Iwata, S. (1982) River terraces along the middle Kali Gandaki and Marsyandi Khola, central Nepal. *Journal of the Nepal Geological Society*, **2**, 95–112.
- Zeitler, P.K. (1985) Cooling history of the NW Himalaya, Pakistan. *Tectonics*, **4**, 127–151.
- Zeitler, P.K., Meltzer, A.S., Koons, P.O., Craw, D., Hallet, B., Chamberlain, C.P., Kidd, W.S.F., Park, S.K., Seeber, L., Bishop, M. and Shroder, J. (2001) Erosion, Himalayan Geodynamics, and the Geomorphology of Metamorphism. *Geological Society of America Today*, **11**, 4–9.
- [Manuscript received sometime:
revised when]